Published for SISSA by Springer

Received: November 15, 2023
Revised: February 19, 2024
Accepted: February 23, 2024
Published: April 2, 2024

Polarised cross sections for vector boson production with Sherpa

Mareen Hoppe[a], **Marek Schönherr**[b] **and Frank Siegert**[a]

[a] *Institute for Nuclear and Particle Physics, TUD Dresden University of Technology, Zellescher Weg 19, D–01062 Dresden, Germany*

[b] *Institute for Particle Physics Phenomenology, Department of Physics, Durham University, Durham, DH1 3LE, U.K.*

E-mail: mareen.hoppe@tu-dresden.de, marek.schoenherr@durham.ac.uk, frank.siegert@cern.ch

Abstract: Measurements of vector boson polarisation in vector boson production processes offer a powerful probe of the electroweak symmetry breaking mechanism, scrutinising the Standard Model and new physics scenarios alike. Since massive vector bosons can only be observed as intermediate particles, polarised cross section templates from simulation are necessary to extract their polarisation from measurable unpolarised distributions. In this work we present an extension of the Sherpa Monte-Carlo event generator allowing the simulation of polarised cross sections for vector boson production processes. Based on the narrow-width approximation, polarised cross sections of all possible polarisation combinations for an arbitrary number of intermediate vector bosons can be simulated in a single simulation run. In addition, it is possible to directly predict the interference between different intermediate polarisation states, and various differing polarisation definitions can be studied simultaneously. Besides the simulation of polarised cross sections at fixed LO and LO+PS accuracy as well as in multijet-merged calculations, we also present parton-shower-matched polarised cross sections with approximate NLO QCD corrections in the vector boson production processes. We demonstrate that the differences of this approximation to full NLO QCD predictions are small and it thus opens up the possibility for fully-simulated calculations at the hadron level including polarisation information and higher-order QCD effects for the first time.

Keywords: Parton Shower, Specific QCD Phenomenology

ArXiv ePrint: 2310.14803

https://doi.org/10.1007/JHEP04(2024)001

JHEP04(2024)001

Contents

JHEP04(2024)001

1 Introduction

The investigation of the polarisation of massive vector bosons (VB) has gained significant attention in recent years, both theoretically and experimentally. The longitudinal polarisation of massive VBs is a direct consequence of the electroweak symmetry breaking mechanism, making polarised VB production a very promising group of processes for probing this mechanism. Similarly, the diagrams of many VB production processes contain triple and quartic gauge coupling vertices, which further contribute to their significance as probes for the innermost gauge symmetry structure of the Standard Model (SM). In addition, measurements of VB polarisation have the potential to provide insights into physics beyond the Standard Model (BSM). In such models, for example, modifications in the VB scattering (VBS) cross sections of longitudinally polarised $W^{\pm}$ and Z bosons can arise due to different Higgs boson couplings to gauge bosons or the presence of new resonances [1, 2]. Some new physics models even predict differences in the VBS cross sections of transversely polarised $W^{\pm}$ and Z bosons [3].

First VB polarisation measurements at the LHC are conducted with data from collisions at 7 and 8 TeV center-of-mass energy (CME) for $W^{\pm}$ boson+jet and Z boson+jet production [4–8] as well as in top quark decays [9–11]. Data taken from the recently finished Run 2 of the LHC at 13 TeV CME is currently being analysed. First measurements are presented for $W^{\pm}Z$ production [12–14] and $W^{\pm}W^{\pm}$ scattering [15]. The expected high luminosity in the forthcoming LHC-runs will provide higher sensitivity to VB polarisation and will also enable polarisation measurements of very rare processes such as the various VBS modes [16, 17].

Since massive VBs only appear as intermediate particles in observable processes, VB polarisation measurements require polarised cross section templates provided by Monte Carlo (MC) event generators to extract polarisation information from the unpolarised, measurable data. Currently, only a few generators are able to separate polarisation states on amplitude level: the MadGraph [18, 19] matrix element generator is able to simulate polarised cross sections for general multi-boson processes at leading order (LO) and interface these to parton shower programs like Pythia [20] and Herwig [21, 22]. The MC event generator Phantom [23] can provide LO polarised predictions for $2 \to 6$ processes. With Recola [24, 25] and Collier [26], the generation of polarised events has been extended to next-to-leading order (NLO) QCD for diboson-production processes in fully- and semi-leptonic decay channels [27–30] and to NLO EW in Z boson pair production [29]. For $W^{\pm}$ boson+jet- and $W^{+}W^{-}$ boson production predictions up to NNLO QCD [31, 32], for inclusive $W^{\pm}Z$ boson pair production up to NLO QCD+EW [33–35] are available.

The framework introduced in this work enables the simulation of polarised cross sections for unstable VBs with the general-purpose MC event generator Sherpa [36]. It thus provides a second fully realistic prediction at the hadron level including effects of parton showers and hadronisation. Polarised cross sections of all possible polarisation combinations can be computed in one simulation run and are provided as additional event weights in Sherpa. Furthermore, the interference between different polarisations can be calculated directly without relying on histogram subtraction methods, and several polarisation definitions are provided. The implementation relies on tree-level matrix elements for multi-leg matrix elements, and it is shown that these can be utilised to simulate the majority of the effect on VB polarisations at NLO QCD with Sherpa if the influence of virtual corrections on polarisation fractions is negligible.

This paper is organised as follows. In section 2, the definition of polarisation for intermediate VBs is introduced. Implementation details of the new polarisation framework in Sherpa are presented in section 3, also covering how the simulation of VB polarisation aspects at NLO QCD becomes possible. The implementation is validated against literature data at fixed LO for several processes in section 4. First applications of the new framework in phenomenological analyses investigating higher-order QCD corrections to polarised cross sections are discussed in section 5. Finally, section 6 gives a summary of this work and an outlook into future extensions of the new framework and planned applications.

2 Definition of polarised amplitudes for intermediate vector bosons

In this section we introduce the definition of the polarisation of intermediate massive VBs. The production of a single massive VB and its subsequent decay into a fermion pair is

JHEP04(2024)001

described in unitary gauge by the amplitude,

$$\mathcal{M} = \mathcal{M}_\mu^{\text{prod}} \left(\frac{i \left(-g^{\mu\nu} + \frac{q^\mu q^\nu}{m_V^2} \right)}{q^2 - m_V^2 + i\Gamma_V m_V} \right) \mathcal{M}_\nu^{\text{decay}} , \tag{2.1}$$

with m_V, Γ_V and q^μ denoting mass, width and four-momentum of the intermediate VB.

This amplitude is connected with the VB polarisation, described by four polarisation vectors $\varepsilon_\lambda^\mu(q)$, via the completeness relation

$$\left(-g^{\mu\nu} + \frac{q^\mu q^\nu}{m_V^2} \right) = \sum_{\lambda=1}^{4} \varepsilon_\lambda^\mu(q) \varepsilon_\lambda^{*\nu}(q) . \tag{2.2}$$

This sum contains the three physical polarisation states, two transverse and one longitudinal, and a fourth unphysical polarisation which only vanishes for on-shell states.[1] The three physical polarisation vectors have the properties,

$$q_\mu \cdot \varepsilon_\lambda^\mu(q) = 0 \qquad\qquad \varepsilon_\lambda^\mu(q) \cdot \varepsilon_{\mu,\lambda'}^*(q) = -\delta_{\lambda\lambda'} . \tag{2.3}$$

Their form depends on the chosen spin basis. For an on-shell massive VB with momentum $q^\mu = (q^0, |\vec{q}| \cos\phi \sin\theta, |\vec{q}| \sin\phi \sin\theta, |\vec{q}| \cos\theta)$ considered in a helicity basis, they are given by

$$\begin{aligned} \varepsilon_\pm^\mu(q) &= \frac{e^{\pm i\phi}}{\sqrt{2}} (0, -\cos\theta\cos\phi \pm i\sin\phi, -\cos\theta\sin\phi \mp i\cos\phi, \sin\theta) , \\ \varepsilon_0^\mu(q) &= \frac{q^0}{m_V} \left(\frac{|\vec{q}|}{q^0}, \cos\phi\sin\theta, \sin\phi\sin\theta, \cos\theta \right) . \end{aligned} \tag{2.4}$$

Besides this four-vector representation, the polarisation vectors can also be expressed in terms of Weyl spinors. The polarisation vectors implemented in Sherpa's built-in matrix-element generator Comix [38] take the form [39]

$$\varepsilon_{+,\dot{A}B}(q) = \frac{\sqrt{2} a_{\dot{A}} b_B}{\langle ab \rangle^*} \qquad \varepsilon_{-,\dot{A}B}(q) = \frac{\sqrt{2} b_{\dot{A}} a_B}{\langle ab \rangle} \qquad \varepsilon_{0,\dot{A}B}(q) = \frac{1}{m_V} (b_{\dot{A}} b_B - \alpha a_{\dot{A}} a_B) . \tag{2.5}$$

a_A and b_A are Weyl spinors which corresponds to the light-like four-vectors in the decomposition of the VB momentum $q^\mu = \alpha a^\mu + b^\mu$ with $\alpha = \frac{q^2}{2a\cdot q}$ necessary to express four-vectors in terms of those spinors. The four-vector a^μ can generally be chosen arbitrarily, however, for massive particles it takes on a physically meaningful role as it fixes the spin axis s^μ of the particle [40]

$$s^\mu = \frac{1}{m} (q^\mu - 2\alpha a^\mu) . \tag{2.6}$$

The helicity basis is obtained by setting $a^\mu \propto (1, -\vec{q}/|\vec{q}|)$ which results in a spin vector pointing in the direction of $\vec{q}$

$$s_\text{hel}^\mu = \frac{1}{m} \left(|\vec{q}|, q^0 \frac{\vec{q}}{|\vec{q}|} \right) . \tag{2.7}$$

[1] The fourth polarisation does also not contribute if the intermediate VB decays into massless leptons [37].

JHEP04(2024)001

Then, polarisation vectors calculated in Sherpa have the form of eq. (2.4) after transforming them back to the four-vector representation. At this point it is paramount to note that the representations of polarisation vectors in eqs. (2.4) and (2.5) are not Lorentz-covariant, $\Lambda^\mu{}_\nu \varepsilon^\nu(q,\lambda) \neq \varepsilon^\mu(\Lambda q,\lambda)$. Consequently, the polarisation of a particle depends on the frame in which its polarisation vectors are calculated.

Out of all possible reference frames (at least) two different frames can now be distinguished to be useful in polarisation measurements — the laboratory rest frame and the rest frame of the massive VBs. Of course, the polarisation vectors obtained in one frame differ from those that are obtained in the other, and contributions of the individual polarisations to the (invariant) unpolarised cross section of the whole process are thus frame dependent. This fact is used in experimental analyses [12, 15] to maximise or minimise the contribution of the interesting polarisations.

Since massive VBs only appear as intermediate, off-shell particles in measurable processes, their polarisation can only be deduced from the distributions of their final state decay products. For fully leptonic decays, massless leptons and no applied lepton selection criteria, an analytical equation for the angular distribution of the $\mathrm{W}^\pm$/ Z boson decay products as a function of the lepton decay angle[2] exists which allows for a determination of the polarisation fractions by projecting the angular distribution on Legendre polynomials [37, 41].

However, in realistic setups, lepton selection criteria need to be applied. They spoil the factorisation of the angular dependence which is necessary to derive this angular distribution. Hence, to measure polarisation fractions in realistic setups, polarised cross sections need to be simulated.

The fact that VBs are only present as intermediate particles leads to two difficulties in the definition of polarised cross sections which would not arise for external VBs. The first one is a direct consequence of eq. (2.2): by inserting eq. (2.2) into eq. (2.1), the matrix element can be factorised into the production and decay of an on-shell VB

$$\begin{aligned}\mathcal{M} &= \frac{i}{q^2 - m_\mathrm{V}^2 + i\Gamma_\mathrm{V} m_\mathrm{V}} \sum_\lambda \mathcal{M}_\mu^\mathrm{prod} \varepsilon_\lambda^{*\mu} \varepsilon_\lambda^\nu \mathcal{M}_\nu^\mathrm{decay} \\ &= \frac{i}{q^2 - m_\mathrm{V}^2 + i\Gamma_\mathrm{V} m_\mathrm{V}} \sum_\lambda \mathcal{M}_\lambda^\mathcal{P} \mathcal{M}_\lambda^\mathcal{D} =: \sum_\lambda \mathcal{M}_\lambda^\mathcal{F} \,,\end{aligned} \tag{2.8}$$

with $\mathcal{M}_\lambda^\mathcal{F}$ being the complete amplitude containing a single VB with definite polarisation λ, and $\mathcal{M}_\lambda^\mathcal{P}$ and $\mathcal{M}_\lambda^\mathcal{D}$ being the respective production and decay amplitudes. Squaring this yields

$$\underbrace{|\mathcal{M}|^2}_{\text{coherent sum}} = \underbrace{\sum_\lambda |\mathcal{M}_\lambda^\mathcal{F}|^2}_{\text{polarised contributions, incoherent sum}} + \underbrace{\sum_{\lambda\neq\lambda'} \mathcal{M}_\lambda^\mathcal{F} \mathcal{M}_{\lambda'}^{*\mathcal{F}}}_{\text{interference}} \,, \tag{2.9}$$

where not only transition matrix elements with intermediate VBs of definite polarisation contribute, but also interferences between different VB polarisation states emerge. These additional interference contributions are generally non-negligible, and only vanish in the

[2]The (lepton) decay angle θ^* is defined as the angle between the charged lepton's momentum in the VB rest frame and the VB's flight direction in the reference frame used for polarisation definition, the VB rest frame is reached by boosting the charged lepton's momentum from the reference frame.

JHEP04(2024)001

absence of lepton selection criteria [37]. Otherwise, they need to be considered as an additional part of the polarisation measurement. Unless stated otherwise, when discussing "interference" in the following, this will always refer to this interference contribution between different polarisations. Likewise, "polarised contributions" form the incoherent sum of the contributions with definite VB polarisation states in eq. (2.9).

The second difficulty arises if more complicated processes are considered involving at least two intermediate bosons. Not all diagrams participating in VB pair production processes exclusively contain final state leptonic lines connected to a single VB each, e.g. double-resonant diagrams for processes with two intermediate VBs as exemplified in figure 1. For not fully-resonant diagrams, e.g. non- and single-resonant diagrams in the boson pair case and denoted "non-resonant contributions" in the following, the definition of polarisation for all intermediate VBs is unfeasible, since they cannot be interpreted as VB production times decay. Simply ignoring these diagrams would break electroweak gauge invariance. Thus, suitable approximations are necessary which allow to omit these diagrams while retaining gauge invariance at the same time. Two common approximations which fulfil these requirements are described below.

- **Narrow-Width Approximation (NWA)** is the approximation utilised by Sherpa and MadGraph. It mainly replaces the denominator of the propagator by a delta function such that only on-shell contributions remain:

$$\frac{1}{q^2 - m_V^2 + i\Gamma_V m_V} \to \frac{\pi}{m_V \Gamma_V} \delta(q^2 - m_V^2)\,. \tag{2.10}$$

- **(Double[3]-)Pole Approximation (DPA)** is used by several MC event generators such as Phantom [23]. It partially considers off-shell effects by only projecting the numerator of the propagator to on-shell momenta while leaving the denominator unchanged. This projection is not unique since sending the intermediate VBs to mass-shell requires at least the adjustment of its decay products' momenta. Further details about this approximation can be found, e.g., in ref. [37]. In the literature, the DPA is often also referred to as On-Shell projection technique (OSP).

The accuracy of both approximations is of order $\mathcal{O}(\Gamma_V/m_V)$ [31, 41]. The final amplitudes result from inserting the completeness relation into the VB propagators and applying one of the approximations above, factorising them into production and decay matrix elements of external, on-shell VBs $\mathcal{M}^{\mathcal{P}}_{\lambda_1,\ldots,\lambda_n}$ and $\mathcal{M}^{\mathcal{D}}_{\lambda_i}$:

$$\begin{aligned}\mathcal{M}_{\text{approx}} &\propto \sum_{\lambda_1\ldots\lambda_n} \mathcal{M}^{\text{prod}}_{\mu_1\ldots\mu_n} \varepsilon^{*\mu_1}_{\lambda_1} \cdots \varepsilon^{*\mu_n}_{\lambda_n} \varepsilon^{\nu_1}_{\lambda_1} \cdots \varepsilon^{\nu_n}_{\lambda_n} \mathcal{M}^{\text{decay}}_{\nu_1} \cdots \mathcal{M}^{\text{decay}}_{\nu_n} \\ &= \sum_{\lambda_1\ldots\lambda_n} \mathcal{M}^{\mathcal{P}}_{\lambda_1\ldots\lambda_n} \mathcal{M}^{\mathcal{D}}_{\lambda_1} \cdots \mathcal{M}^{\mathcal{D}}_{\lambda_n}\,.\end{aligned} \tag{2.11}$$

If both factors are gauge invariant, this also holds for the overall approximated matrix element. Since the VBs are on-shell in the polarisation dependent part of the matrix element

[3]The pole approximation is also called double-pole approximation for the case of VB pair production processes.

JHEP04(2024)001

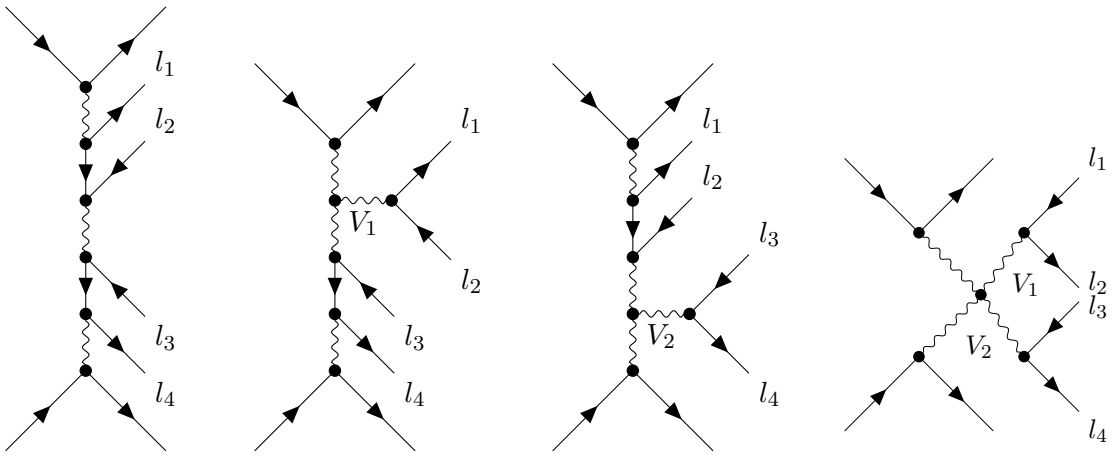

Figure 1. Categories of diagrams contributing to vector boson production processes with vector bosons V_1, V_2 decaying into leptons l_1, l_2 or l_3, l_4.

in both approximations, the unphysical auxiliary polarisation does not contribute so that each term of the polarisation sum in eq. (2.11) provides a physical polarisation contribution to the process of interest.

3 Simulation of polarised cross sections

3.1 Basic concepts

In order to simulate polarised cross sections, amplitudes containing different VB polarisations need to be separated as detailed in the previous section. In Sherpa, such amplitudes are available as intermediate results within the framework for simulating heavy resonances in the NWA [42]. For that, the VB are produced on-shell and are subsequently decayed by an implementation of the spin-correlation algorithm introduced in ref. [43]. In order to at least partly recover kinematic off-shell effects of the total process, a smearing of the intermediate VB's invariant mass according to its Breit-Wigner distribution is performed after their generation, affecting only the kinematics of the final state particles. The matrix elements remain unchanged, i.e., calculated in NWA with on-shell VBs.

The main input for the spin correlation algorithm is an amplitude tensor containing all production matrix elements as a function of the VB polarisations (production tensor), $|\mathcal{M}^{\mathcal{P}}|^2_{\lambda_1\ldots\lambda_n,\lambda'_1\ldots\lambda'_n}$. During the simulation of the decay (cascade), a decay matrix $D_{\lambda_i\lambda'_i}$ is calculated for each particle. Following from eq. (2.11), they are defined through

$$\begin{aligned} |\mathcal{M}^{\mathcal{F}}|^2_{\lambda_1\ldots\lambda_n,\lambda'_1\ldots\lambda'_n} &= \mathcal{M}^{\mathcal{P}}_{\lambda_1\ldots\lambda_n}\mathcal{M}^{*\mathcal{P}}_{\lambda'_1\ldots\lambda'_n}\mathcal{M}^{\mathcal{D}}_{\lambda_1}\mathcal{M}^{*\mathcal{D}}_{\lambda'_1}\cdots\mathcal{M}^{\mathcal{D}}_{\lambda_n}\mathcal{M}^{*\mathcal{D}}_{\lambda'_n} \\ &= N\cdot|\mathcal{M}^{\mathcal{P}}|^2_{\lambda_1\ldots\lambda_n,\lambda'_1\ldots\lambda'_n}\prod_{i=1}^{n}D_{\lambda_i\lambda'_i}\,. \end{aligned} \tag{3.1}$$

The normalisation constant N is the product of the normalisation constants of all decay matrices $N=\prod_{i=1}^{n}n_i$ with $n_i=\mathcal{M}^{\mathcal{D}}_{\lambda_i;\rho_1\ldots\rho_m}\mathcal{M}^{*\mathcal{D}}_{\lambda'_i;\rho'_1\ldots\rho'_m}\prod_{j=1}^{m}D^{j}_{\rho_j,\rho'_j}$ being the normalisation

JHEP04(2024)001

constant of the decay matrix of the ith VB and $D^j_{\rho_j,\rho'_j}$ denoting the decay matrices of the m decay products of the respective VB. The constant n_i ensures that the trace of each decay matrix $D_{\lambda_i\lambda'_i}$ is one.[4]

The spin basis used for matrix element calculation in Sherpa's built-in matrix element generator Comix (default polarisation basis) is not the helicity basis, which is typically assumed for VB polarisation measurements, but uses constant universal reference vectors. Furthermore, other reference systems than the laboratory frame used per default may be interesting, e.g. to maximise the longitudinal contribution of the VBs. Hence, a transformation of polarisation definitions from one frame to another is needed.

Such a change amounts to a change of basis in the polarisation definitions, and, hence, polarisation objects (spinors, polarisation vectors) defined in one basis can be expressed as a linear combination of polarisation objects obtained in another basis. By replacing the polarisation objects defined in the desired polarisation definition in basis $\tilde{A}$ in the corresponding matrix elements by the linear combination of the polarisation objects in basis A used in the matrix element calculation, the following transformation is obtained

$$|\mathcal{M}|^2_{\lambda_1\ldots\lambda_n,\lambda'_1\ldots\lambda'_n}\Big|_{\tilde{A}} = \sum_{\kappa_1\ldots\kappa_n,\kappa'_1\ldots\kappa'_n} a^{\pi_1}_{\lambda_1,\kappa_1} a^{*\pi_1}_{\lambda'_1,\kappa'_1}\cdots a^{\pi_n}_{\lambda_n,\kappa_n} a^{*\pi_n}_{\lambda'_n,\kappa'_n}\, |\mathcal{M}|^2_{\kappa_1\ldots\kappa_n,\kappa'_1\ldots\kappa'_n}\Big|_{A}\,, \tag{3.2}$$

with λ_i (κ_i) describing the polarisations of the ith particle π_i in the desired (default) polarisation definitions. The transformation coefficient $a^{\pi_i}_{\lambda_i,\kappa_i}$ is the linear combination coefficient for polarisation κ_i within the polarisation object in the matrix element with polarisation λ_i. The $a^{*\pi_i}_{\lambda'_i,\kappa'_i}$ are the corresponding linear combination coefficients for the complex conjugate matrix elements. $|\mathcal{M}|^2_{\kappa_1\ldots\kappa_n,\kappa'_1\ldots\kappa'_n}$ denotes either the production tensor or a decay matrix, in the respective polarisation basis. The linear combination coefficients can be determined by solving the system of equation

$$\underbrace{\begin{pmatrix} \tilde{\varepsilon}^1_+ & \tilde{\varepsilon}^1_- & \tilde{\varepsilon}^1_0 \\ \tilde{\varepsilon}^2_+ & \tilde{\varepsilon}^2_- & \tilde{\varepsilon}^2_0 \\ \tilde{\varepsilon}^3_+ & \tilde{\varepsilon}^3_- & \tilde{\varepsilon}^3_0 \end{pmatrix}}_{\substack{\text{polarisation vectors in} \\ \text{polarisation basis } \tilde{A}}} = \underbrace{\begin{pmatrix} \varepsilon^1_+ & \varepsilon^1_- & \varepsilon^1_0 \\ \varepsilon^2_+ & \varepsilon^2_- & \varepsilon^2_0 \\ \varepsilon^3_+ & \varepsilon^3_- & \varepsilon^3_0 \end{pmatrix}}_{\substack{\text{polarisation vectors in} \\ \text{polarisation basis } A}} \underbrace{\begin{pmatrix} a_{++} & a_{+-} & a_{+0} \\ a_{-+} & a_{--} & a_{-0} \\ a_{0+} & a_{0-} & a_{00} \end{pmatrix}}_{\substack{\text{linear combination} \\ \text{coefficients}}}, \tag{3.3}$$

by inversion. For the inverse of a (3x3) matrix an analytical formula exists, so no numerical determination is necessary. Note that the zeroth component of the polarisation vector is omitted in eq. (3.3) since not all components of a polarisation vector are independent according to eq. (2.3).

3.2 Structure of the new polarisation framework

Following the ideas and concepts introduced in the previous section, the event generation for processes with heavy resonances in NWA remains unchanged if polarised cross sections should be simulated. Only copies of the production tensor and the decay matrices are made

[4] In cases where the decay products of VB i decay further, the decay tensor $D_{\lambda_i\lambda'_i}$ is replaced (iteratively in case of longer decay cascades), up to a normalisation constant, by $D_{\lambda_i\lambda'_i;\rho_1\ldots\rho_m,\rho'_1\ldots\rho'_m}\prod_{j=1}^m D^j_{\rho_j\rho'_j}$ with $\rho^{(\prime)}_j$ being the polarisation indices of the initial VB's decay products.

JHEP04(2024)001

before they are contracted with each other to result in the unpolarised cross section in NWA. In practical terms, the polarised cross sections are provided simultaneously via additional event weights in each event. Those are calculated directly from the matrix elements by

1. **Transformation** of the polarised production tensor and decay matrices to get matrix elements defined in the polarisation basis of interest according to eq. (3.2)
2. **Multiplying** production tensor and decay matrices according to eq. (3.1)
3. **Labelling/Identification** of tensor entries according to the polarisation combinations of interest
4. **Normalisation** to the tensor sum to obtain polarisation fractions.

Those fractions are then multiplied with the nominal event cross section corresponding to the unpolarised cross section of the current event in NWA and stored as event weights. Details about provided weights and their naming scheme can be found in appendix A.2.

This approach enables the simulation of polarised cross sections of all possible polarisation combinations in a single simulation run. Furthermore, the interference between different polarisations can be simulated directly by summing over all off-diagonal entries of the amplitude tensor:

$$\underbrace{|\mathcal{M}|^2}_{\text{coherent sum}} = \underbrace{\sum_{\lambda_1 \dots \lambda_n} |\mathcal{M}^{\mathcal{F}}_{\lambda_1 \dots \lambda_n}|^2}_{\text{polarised contributions, incoherent sum}} + \underbrace{\sum_{\lambda_1 \neq \lambda'_1 \dots \lambda_n \neq \lambda'_n} \mathcal{M}^{\mathcal{F}}_{\lambda_1 \dots \lambda_n} \mathcal{M}^{*\mathcal{F}}_{\lambda'_1 \dots \lambda'_n}}_{\text{interference}} . \tag{3.4}$$

Thus, an interference template can be directly provided for polarisation analyses. It can be included as an additional background in polarisation measurements without relying on histogram subtraction methods that can lead to large statistical uncertainties.

All common reference systems for polarisation definitions are supported, including the laboratory, the parton-parton and the center-of-mass frame of all intermediate particles. Due to the a posteriori approach of adjusting the polarisation definition in the matrix elements all polarisation definitions of interest can be simulated within the same run and an extension to other reference systems (and spin bases) than the provided ones is straightforward. The framework can be applied for an arbitrary number of intermediate VBs.

Practical details, the user input syntax to simulate polarised cross sections with Sherpa and a complete list of currently implemented polarisation definitions can be found in a dedicated section of the Sherpa user manual [44]. A short depiction of the input syntax is also given in appendix A.1.

3.3 Calculation of polarised cross sections at nLO QCD with Sherpa

As described in section 3.1, the new polarisation features are based on Sherpa's framework for computing factorised matrix elements of the production and decay of unstable, intermediate particles. This is not limited to LO: the production matrix elements can also include NLO contributions which can in turn be used for the polarisation calculation enabling the simulation of higher-order polarisation effects. We limit ourselves to NLO QCD corrections.

JHEP04(2024)001

The simulation of NLO polarisation effects currently relies on some approximations depending on the event type. As a consequence, while unpolarised NLO+PS matched calculations with Sherpa's S–Mc@Nlo method [45] retain their complete NLO accuracy, the polarisation fractions computed with the following construction can only approximate it. We construct the amplitude tensor $|\mathcal{M}|^2_{\kappa_1\ldots\kappa_n,\kappa'_1\ldots\kappa'_n}$ depending on the event type.

$\mathbb{H}$ **events.** This category comprises both hard well-separated emissions beyond the parton shower starting scale, and process-specific corrections to the universal soft-collinear emission pattern below it. The corresponding amplitude tensor is constructed from the real emission amplitude itself and thus contains all necessary information in the hard-emission regime.

$\mathbb{S}$ **events, resolved emission.** This category comprises the universal soft-collinear radiation pattern the parton shower approximation produces above its infrared cut-off. The corresponding amplitude tensor is again constructed using the complete real emission amplitude. Hence, in combination with the treatment for $\mathbb{H}$-events in this regime the correct polarisation fractions, up to NLO, are used for both soft and hard emissions.

$\mathbb{S}$ **events, unresolved emission.** Finally, this category contains, to NLO accuracy, all unresolved emissions, i.e. emissions below the parton shower infrared cutoff and all virtual corrections. The amplitude tensor is solely constructed using the Born expression and all virtual and ultra-soft and/or -collinear emission corrections thereupon are neglected. As the number of events in this category is generally small, and this construction is used to determine the polarisation fractions in the otherwise fully NLO-accurate unpolarised sample, the error introduced in this way is expected to be small.

This approximation generally yields satisfactory results and will be denoted as nLO in the following.[5] We investigate it in more detail in section 5.

At this point, the scale dependence of our construction w.r.t. exact result should be addressed. The QCD scale variations of the above nLO accurate construction are formally only LO accurate. However, while both α_s and the (unpolarised) PDFs factorise from the polarised Born and real emission matrix elements or amplitude tensors, and hence are universal for both unpolarised cross sections and (each) polarised one, only the virtual correction, owing to the appearance of the renormalisation scale within the renormalised loop amplitude itself, may display different scale-dependences for different polarisation combinations. Further, the factorisation scale dependence of the collinear counterterm for unpolarised PDFs, which we also neglect in the nLO approximation, factorises from the amplitude tensor as well and is thus also universal for all polarised cross sections. Hence, on an event-by-event basis, assuming the polarisation dependence of the virtual correction to be small, which is a prerequisite for the nLO approximation to be meaningful, the (relative) QCD scale variations of the NLO accurate unpolarised cross sections are expected to be a good representation of the scale uncertainties

[5] Extending the polarised matched cross section to full NLO accuracy necessitates the additional availability of the amplitude tensor for the renomalised virtual correction (including collinear counterterms), differential and integrated subtraction terms, and shower splitting kernels for the first/matched emission. While this does not represent an obstacle in principle, its technical implementation is beyond the scope of this paper.

JHEP04(2024)001

Process $\mathcal{O}(\alpha^6)$	Reference	Approximation	Reference system
W^+W^+jj: $pp \to e^+ \nu_e \mu^+ \nu_\mu jj$	[47]	DPA	Lab, COM
W^+W^-jj: $pp \to e^+ \nu_e \mu^- \bar{\nu}_\mu jj$	[47]	DPA	Lab, COM
W^+W^-jj: $pp \to \mu^+ \nu_\mu e^- \bar{\nu}_e jj$	[37]	DPA	Lab
W^+Zjj: $pp \to e^+ \nu_e \mu^+ \mu^- jj$	[47]	DPA	Lab, COM
W^+Zjj: $pp \to \mu^+ \nu_\mu e^+ e^- jj$	[41]	DPA	Lab
$ZZjj$: $pp \to e^+ e^- \mu^+ \mu^- jj$	[47]	DPA	Lab, COM
	[41]	RES NO OSP	Lab

Table 1. Details about the literature studies used to validate the new SHERPA implementation for simulating polarised cross sections for vector boson production processes. Here, DPA denotes the Double-Pole Approximation, RES NO OSP the use of double-resonant diagrams in the full off-shell phase space without any On-Shell Projection (OSP), while Lab signals the use of the laboratory frame, and COM the center-of-mass frame of the VB pair, to define the polarisation states.

of the actual NLO polarised cross sections. Consequently, in our approximation, sourcing the polarisation fractions at nLO only from the Born and real emission amplitude tensors where the QCD scale variations completely factorise, the polarised cross sections all share the same scale uncertainty and the polarisation fractions therefore are scale independent.

A similar phenomenon holds for merged setups of tree-level multi-leg matrix elements. In the matrix element jet production region the full real-emission kinematics is taken into account also for the polarisation calculations and thus the bulk of higher-order QCD corrections for them is included. The same methods can not be reliably applied for NLO EW corrections, or the EW_{virt} approximation [46] for that matter, because there the virtual effects in the production and decay will have a significant impact on VB polarisation fractions.

4 Validation of the implementation at fixed leading order

The SHERPA implementation presented in the previous section is validated by comparing polarised integrated cross sections and differential distributions obtained with the new polarisation framework with literature data for several pure electroweak VB-pair-production processes in association with two jets at fixed leading order ($\mathcal{O}(\alpha^6)$).[6] Table 1 summarises all literature data which is included in this validation study. All considered literature data were obtained with PHANTOM [23] for an LHC beam setup with 13 TeV proton-proton center-of-mass energy assuming SM dynamics, and rely on different approximations to omit single- and non-resonant diagrams than SHERPA. Hence, literature and SHERPA predictions may differ on the order of $\mathcal{O}(\Gamma_V/m_V)$. The VB polarisation is defined in the helicity basis. Simulation parameters and phase space definitions are chosen identical to the literature, for details see also appendix B.1. Typically, two different phase space definitions are distinguished

[6] For simplicity, those processes are abbreviated as VBS processes in this work, even though not only VBS diagrams contribute to them.

JHEP04(2024)001

Process	σ_{PHANTOM} [fb]		σ_{SHERPA} [fb]	
	full	unpol	full	unpol
W^+W^+jj	3.185(3)	3.167(2)	3.1814(13)	3.1839(10)
W^+W^-jj	4.651(2)	4.641(2)	4.631(22)	4.6707(22)
W^+Zjj	0.5253(3)	0.5210(3)	0.5258(11)	0.52471(27)
$ZZjj$	0.1270(1)	0.1264(1)	0.12715(25)	0.12801(10)

Table 2. Integrated full and unpolarised cross sections for several pure electroweak vector boson pair production processes in association with two jets at fixed LO obtained with PHANTOM from ref. [47] and SHERPA in the inclusive phase space defined in section B.1.

in the literature based on whether lepton acceptance criteria are applied (fiducial setup) or not (inclusive setup).

For each investigated process, two simulation runs are done:

- **Full calculation (denoted "full"):** no approximation is applied so that all off-shell effects of the intermediate VBs as well as all effects from single- and non-resonant contributions are retained.

- **Polarised calculation:** SHERPA's spin-correlated narrow-width approximation as introduced in section 3 is used to compute polarised contributions, distinguishing longitudinal (**"L"**), transverse (**"T"**, summing left- and right-handed polarised contributions as well as left-right interference terms) and their *incoherent* sum (**"polsum"**). Furthermore, the unpolarised cross section in the NWA (**"unpol"**) is calculated, which additionally also contains the interferences, i.e. the *coherent* sum of all polarised matrix elements. The unpol differs from the full result by the missing non-resonant contributions and not-completely covered off-shell effects.

Uncertainties reported within this work only take the limited MC statistics into account. There are also systematic uncertainties due to missing higher-order contributions, which could be estimated by scale and PDF variations.

The data generated with SHERPA is analysed via the analysis framework RIVET [48], details are given in appendix B.1.

A first comparison of integrated cross sections is summarised in table 2, which compares the unpolarised predictions obtained with PHANTOM in ref. [47] with those resulting from the new polarisation framework in SHERPA in the inclusive setups. As is evident, SHERPA's NWA leads to a very good approximation of the full result for all investigated processes and phase space regions. Observed deviations are $\ll 1\%$. The difference between the unpolarised results from the literature and SHERPA amounts to 1.3% or less which is fully within the expected accuracy of $\mathcal{O}(\Gamma_V/m_V)$ ($\sim 2.5\%$).

In figure 2, the polarisation fractions for the investigated processes computed with SHERPA in the inclusive setups with polarisation defined in the laboratory (Lab) and the VB pair center-of-mass (COM) frames, respectively, are displayed in comparison with the

JHEP04(2024)001

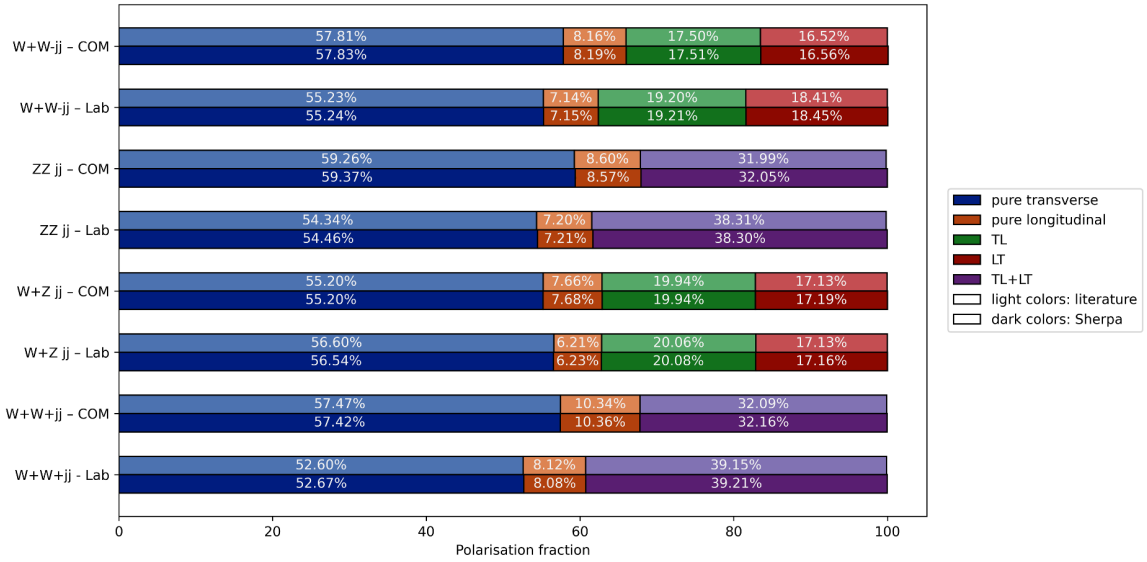

Figure 2. Comparison of polarisation fractions obtained with PHANTOM in ref. [47] and SHERPA for several pure electroweak VB pair production processes in association with two jets at fixed leading order in the inclusive phase space defined in section B.1, vector boson polarisation is defined in the laboratory (Lab) or the vector boson pair center-of-mass frame (COM). Polarisation fractions are computed relative to the unpolarised results indicating vanishing interference between different polarisations as expected in the absence of lepton selection requirements. Statistical uncertainties of the polarisation fractions are of $\mathcal{O}(10^{-2})\%$.

PHANTOM results indicating an excellent agreement with deviations of less than 0.6%. The simulated interference contribution is compatible with zero, as expected when no lepton acceptance criteria are applied.

For a more differential validation a selection of the observables investigated in refs. [37, 41, 47] is reproduced with our new implementation in SHERPA in figures 3–6. The (partially) polarised differential cross sections are computed in the fiducial phase spaces defined in appendix B.1. Resulting integrated cross sections are displayed in tables 8–10 in the appendix B.2 for completeness. They agree within the expected accuracy (deviations <1.5%). Except the W^+W^+jj process, where also results for the polarisation defined in the COM and double-polarised differential cross sections are discussed in the literature, all distributions are computed in the Lab and are single-polarised, i.e. only the polarisations of VBs decaying in the electron channel are considered.

Generally, excellent agreement between PHANTOM and SHERPA calculations is found. Observed deviations are small, far below the expected accuracy due to the different approximations used. Furthermore, it is confirmed that the unpolarised predictions obtained by applying SHERPA's spin-correlated NWA reproduce the full result at a comparable level as the DPA for the investigated processes and phase spaces.

The interference contribution, which, at variance with the literature, our implementation allows to compute directly, has also been added to the presented figures. For most observables and phase space regions studied here the interference is small in comparison

JHEP04(2024)001

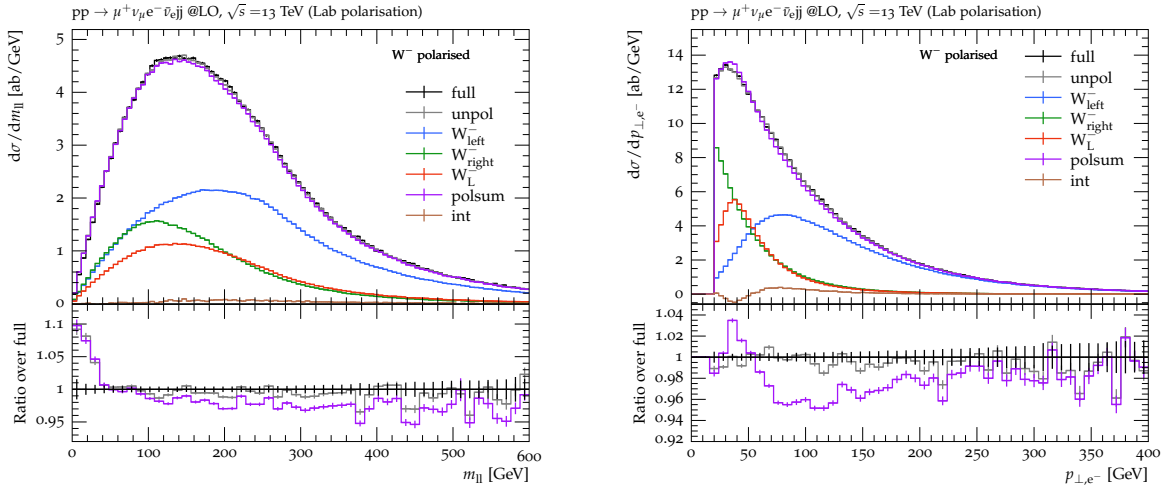

Figure 3. Single-polarised distributions of the charged leptons invariant mass m_{ll} (left) and the transverse momentum of the electron $p_{\perp,e^-}$ for the W^+W^-jj process in the fiducial phase space (details in main text) obtained with SHERPA. The W^+ boson is considered unpolarised, the polarisation of the W^- boson is defined in the laboratory frame (Lab). The SHERPA distributions are in very good agreement with those computed with PHANTOM in ref. [37], figure 6.

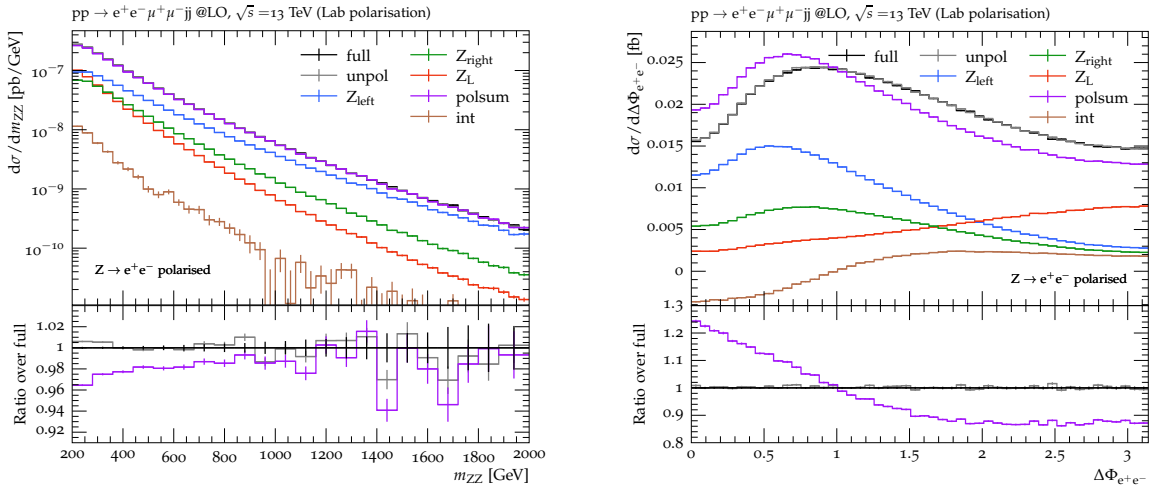

Figure 4. Single-polarised distributions of the ZZ-invariant mass m_{ZZ} (left) and the azimuthal separation $\Delta\Phi_{e^+e^-}$ (right) for the ZZjj process in the fiducial phase space (details in main text) obtained with SHERPA. The Z boson decaying into $\mu^+\mu^-$ is considered as unpolarised, the polarisation of the Z boson decaying into e^+e^- is defined in the laboratory frame (Lab). The ZZ-invariant mass distributions are also computed with PHANTOM in ref. [41], figure 4, the SHERPA distributions shown here are in very good agreement with those.

JHEP04(2024)001

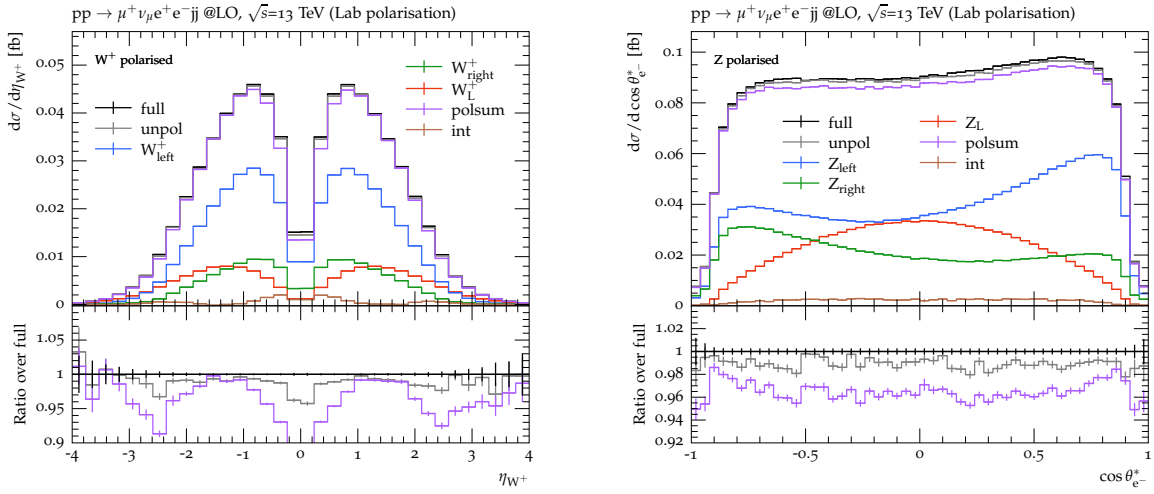

Figure 5. Single-polarised distributions of the W^+ boson pseudorapidity η_{W^+} (left) and the electron decay angle $\cos\theta_{e^-}$ (right) for the W^+Zjj process in the fiducial phase space (details in main text) obtained with SHERPA. The Z boson is considered as unpolarised in the left figure, the W^+ boson in the right figure, the polarisation of the respective polarised boson is defined in the laboratory frame (Lab). The SHERPA distributions are in very good agreement with those computed with PHANTOM in ref. [41], figure 7.

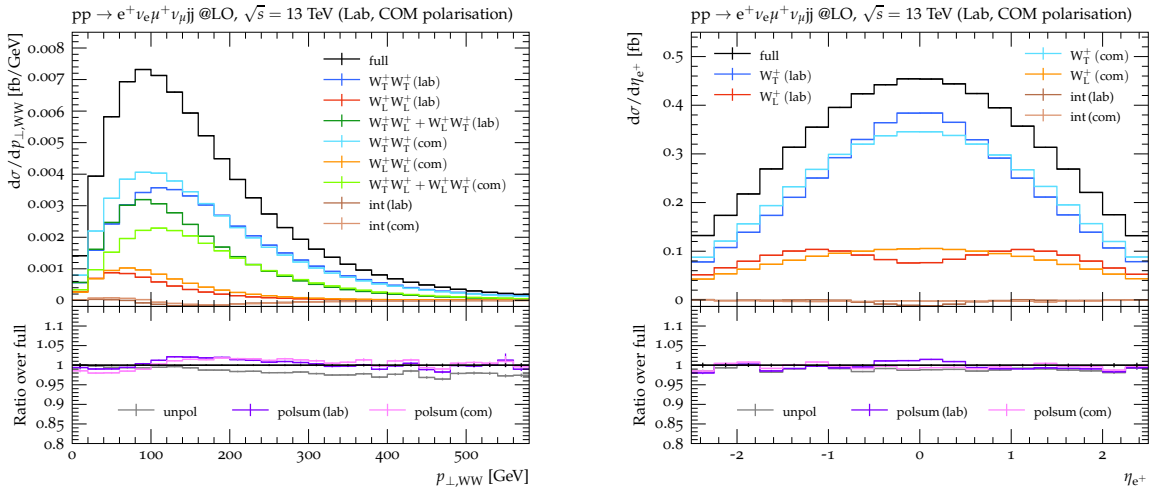

Figure 6. Double-polarised distributions of the W^+W^+ transverse momentum $p_{\perp,WW}$ (left) and single-polarised distributions of the positron pseudorapidity η_{e^+} (right) for the W^+W^+jj process in the fiducial phase space (details in main text) obtained with SHERPA. Polarised differential distributions and the ratios over the full off-shell result are shown in the top respectively bottom graph of each subfigure. For the single-polarised distributions, the W^+ boson decaying into an anti-muon-neutrino pair is considered as unpolarised. Polarisations of both W^+ bosons are defined in the W^+W^+-center-of-mass frame (com) and the laboratory frame (Lab). The SHERPA distributions are in very good agreement with those computed with PHANTOM in ref. [47], figures 2 and 3.

JHEP04(2024)001

to other contributions, amounting to a few percent at most. However, there are also observables where the interference contribution can reach a similar size than the longitudinal contribution in some phase space regions (e.g. around $\eta_{W^+} = 0$ in the W^+Zjj process in figure 5) or can even be very large over large phase space regions (figure 4). It is here, where the direct access to this component facilitates precise measurements of polarised cross sections at any collider experiment.

5 Polarised cross sections beyond leading order

The validation study presented in the previous section reveals a very good agreement between the new Sherpa polarisation framework and the literature for several investigated VB production processes at fixed LO, leading to the conclusion that the new implementation is functional. The inclusion of higher perturbative orders in the hard matrix elements and multijet-merged calculations provide two ways to obtain higher-order corrections to simulated cross sections. As outlined in section 3.3, it is possible to apply the new polarisation framework in Sherpa's NLO calculations. The current implementation, however, leads to polarised predictions at nLO accuracy only, since the calculation of polarisation fractions does not take loop corrections into account. Therefore, the first part of this section focuses on testing, whether the approximation introduced in section 3.3 can nonetheless deliver reliable predictions of the main complete NLO polarisation behaviour. This is done by comparing Sherpa results with full fixed-order NLO calculations from the literature, ref. [28], where predictions with MoCaNlo+Recola+Collier [25, 26] in the DPA are presented. This will be followed by a discussion of the polarised cross sections obtained by combining Sherpa's merging method with the new polarisation framework. In particular, the influence of different merging scales is investigated. We choose inclusive production of a W^+Z boson pair with fully leptonic decays as our testbed.

5.1 Simulation setup

In order to study higher-order predictions with Sherpa in inclusive W^+Z production, simulation settings and the phase space are chosen according to ref. [28]. This allows the comparison with full NLO fixed-order results published there. More specifically, the $pp \to e^+ \nu_e \mu^+ \mu^- + X$ process is studied for an LHC setup with 13 TeV proton-proton center-of-mass energy assuming SM dynamics and using the simulation settings as well as phase space definitions given in table 3. The polarisation is defined in the helicity basis. All leptons and quarks except the top quark are considered to be massless.

Sherpa simulations at nLO+PS accuracy use Born-level matrix elements calculated with Amegic [49], except for the amplitudes employed for the polarisation fraction calculations, the VB decays and calculations at LO. Those amplitudes as well as real corrections are computed with Comix [38]. Virtual corrections are provided by OpenLoops [50] using the Sherpa interface to this program. These simulations showcase a simulation of events including parton shower effects, which allows to interface hadronization models and thus provide a fully-realistic simulation. Since these effects are not taken into account in the reference predictions, one can expect differences in the comparison in particular in regions which become sensitive to

JHEP04(2024)001

PDF-Set from LHAPDF6 [57]	NNPDF31_nlo_as_0118 [58]
Electroweak scheme G_μ	$G_\mu = 1.16638 \cdot 10^{-5}\,\text{GeV}^{-2}$ and complex mass scheme (full), real EW parameters (polarisation)
Strong coupling $\alpha_S(M_\text{Z})$	0.118
Core-Scale	$\mu{=}\frac{1}{2}(M_\text{Z} + M_\text{W})$
VB pole masses	$M_\text{W} = 80.352$ GeV, $M_\text{Z} = 91.153$ GeV
VB pole widths	zero for all VBs in polarisation calculations [37], $\Gamma_\text{W} = 2.084$ GeV, $\Gamma_\text{Z} = 2.4943$ GeV otherwise
Phase space	$p_{\perp,\text{e}^+} > 20\,\text{GeV}$, $p_{\perp,\mu^\pm} > 15\,\text{GeV}$, $\lvert y_\text{l}\rvert < 2.5$
	$\Delta R_{\mu^+\mu^-} > 0.2$, $\Delta R_{\mu^\pm\text{e}^+} > 0.3$
	$81\,\text{GeV} < M_{\mu^+\mu^-} < 101\,\text{GeV}$, $M_{T,\text{W}} > 30\,\text{GeV}$

Table 3. Settings and phase space definition used for the inclusive W^+Z production at nLO+PS and LO+1j merged calculations. The transverse mass is defined as $M_{T,\text{W}} = \sqrt{2p_{\perp,\text{e}^+}p_{\perp,\nu_\text{e}}(1-\cos\Delta\phi_{\text{e}^+\nu_\text{e}})}$.

resummation. The matching of the fixed-order NLO calculation to the resummation of the parton shower is done by Sherpa's internal implementation of the Mc@Nlo method [45]. The core-scale of the processes is set by Sherpa's METS-scale setter [51].

Merged calculations with Sherpa in this section investigate the $\text{pp} \to \text{e}^+\,\nu_\text{e}\,\mu^+\,\mu^-$ process merged with $\text{pp} \to \text{e}^+\,\nu_\text{e}\,\mu^+\,\mu^-\text{j}$ at LO. All matrix elements are provided by Comix. The merging algorithm implemented in Sherpa is an extension of the CKKW method [52] as detailed in ref. [51] (called MEPS@LO). The merging scale is varied in an extreme range between 20 and 1000 GeV for instructive purposes.

All Sherpa simulations performed in this section apply Sherpa's default shower simulation [53], QED radiation [54], hadronisation [55], hadron decays and multiple interactions [36, 44]. QCD jets are identified by the anti-k_t algorithm [56] with a jet resolution parameter of $R = 0.4$.

The simulation data is analysed with a Rivet analysis based on the ATLAS analysis of ref. [12]. Selection criteria applied during the event generation are set more inclusive than in table 3. The more stringent selection criteria detailed in table 3 are then applied on the reconstructed final state jets and dressed final state leptons at the analysis stage. We then focus on double-polarised cross sections.

The labels for the different types of calculations (full off-shell, NWA) and polarised contributions are the same as in the previous section.

5.2 Polarised cross sections at nLO+PS

Table 4 compares the integrated polarised cross sections obtained with Sherpa's nLO+PS polarisation setup with the literature results of ref. [28] containing all NLO corrections at fixed order. For completeness, also single-polarised cross sections are displayed. Both the laboratory (Lab) as well as the W^+Z-center-of-mass reference frame (COM) are investigated. NLO corrections in W^+Z production can be very large with K-factors around two. This is

JHEP04(2024)001

W^+Z	σ^{NLO} [fb]	Fraction [%]	K-factor	$\sigma^{\text{nLO+PS}}_{\text{SHERPA}}$ [fb]	Fraction [%]	K-factor
full	35.27(1)		1.81	33.80(4)		
unpol	34.63(1)	100	1.81	33.457(26)	100	1.79
			Laboratory frame			
L-U	8.160(2)	23.563(9)	1.93	7.962(5)	23.796(25)	1.91
T-U	26.394(9)	76.217(34)	1.78	25.432(21)	76.01(9)	1.75
int	0.066(10) (diff)	0.191(29)	2.00	0.064(7)	0.191(22)	2.40(40)
U-L	9.550(4)	27.577(14)	1.73	9.275(16)	27.72(5)	1.72
U-T	25.052(8)	72.342(31)	1.83	24.156(18)	72.20(8)	1.81
int	0.028(10) (diff)	0.081(29)	-0.49	0.026(7)	0.079(22)	-0.471(34)
L-L	2.063(1)	5.9573(33)	1.91	2.0128(18)	6.016(7)	1.90
L-T	6.108(2)	17.638(8)	1.93	5.958(5)	17.807(20)	1.91
T-L	7.409(4)	21.395(13)	1.69	7.185(12)	21.47(4)	1.68
T-T	18.964(7)	54.762(26)	1.80	18.215(16)	54.44(6)	1.77
int	0.086(13) (diff)	0.248(35)	-2.97	0.087(7)	0.259(20)	-2.7(4)
			W^+Z-center-of-mass-frame			
L-U	7.308(2)	21.103(8)	2.09	7.132(5)	21.316(22)	2.08
T-U	27.14(1)	78.371(37)	1.75	26.153(17)	78.17(8)	1.73
int	0.182(10) (diff)	0.526(29)	1.28	0.173(10)	0.516(30)	1.30(4)
U-L	7.137(2)	20.609(8)	2.07	6.976(5)	20.850(22)	2.07
U-T	27.449(9)	79.264(35)	1.75	26.441(26)	79.03(10)	1.72
int	0.044(10) (diff)	0.127(29)	∞	0.041(4)	0.122(13)	-15(8)
L-L	1.968(1)	5.6829(33)	1.31	1.9018(19)	5.684(7)	1.28
L-T	5.354(1)	15.461(5)	2.65	5.241(4)	15.665(17)	2.65
T-L	5.097(2)	14.718(7)	2.68	5.002(4)	14.951(16)	2.69
T-T	21.992(9)	63.506(32)	1.62	21.098(16)	63.06(7)	1.59
int	0.219(13) (diff)	0.632(38)	1.54	0.215(9)	0.641(26)	1.65(5)

Table 4. Integrated single- and double-polarised cross sections for the inclusive W^+Z production including higher order QCD corrections in the phase space defined in table 3 obtained with MoCaNlo+Recola+Collier [25, 26] in ref. [28] (full fixed-order NLO correction) and Sherpa (nLO+PS) for polarisations defined in the laboratory and W^+Z-center-of-mass frame; polarisation fractions are calculated relative to the unpolarised result, K-factors are obtained by dividing the NLO (nLO+PS) cross sections by the LO (LO+PS) ones which lead to statistical errors of $\mathcal{O}(10^{-3})$, except for the interference ($\mathcal{O}(10^{-1})$).

JHEP04(2024)001

due to both new flavour channels opening at NLO and the approximate radiation amplitude zero, present at Born level, being filled by NLO real-emission corrections [28].

Comparing the unpolarised Sherpa result with the literature results, while full agreement was observed at LO, the unpolarised Sherpa cross section @nLO+PS is about 3.4% smaller than the literature value. This discrepancy is caused by parton shower and QED effects which are accounted for in the Sherpa calculation but not in the fixed-order reference result and by the different on-shell approximations used. The Sherpa unpolarised result approximates the full cross section better than 1.5%, implying that Sherpa's NWA provides a good approximation to the full result also at NLO.

More interestingly, the polarisation fractions show an agreement of better than 1.5%. This is smaller than the expected accuracy due to the different on-shell approximations used in the two calculations, and the inherent approximation of the nLO calculation used in Sherpa. This leads to the conclusion that virtual corrections do not seem to have a significant influence on the polarisation fractions and Sherpa's nLO setup captures the relevant part of the NLO corrections. It is particularly promising that the differing behaviour in both reference frames is reproduced accurately.

Figures 7 and 8 show the distributions for the decay angle of the anti-muon $\cos\theta^*_{\mu^+}$, the positron rapidity y_{e^+}, the azimuthal angle between the positron and the muon $\Delta\Phi_{e^+\mu^-}$ and the muon transverse momentum $p_{\perp,\mu^-}$ obtained with Sherpa for the Lab and COM polarisation definition. The unpolarised (unpol) distributions approximate the full predictions (full) well, mostly showing deviations of about 2–3% or less. Hence, off-shell and non-resonant effects are small.

The NLO corrections show a strong sensitivity to the polarisation states under consideration, and can be very non-uniform across a given observable, e.g. y_{e^+} with polarisation states defined in the Lab frame. Additionally, shape and size of the NLO corrections for a certain polarisation state can strongly depend on the frame in which the respective polarisation states are defined. Here, the distributions of $\cos\theta^*_{\mu^+}$ or, again, y_{e^+} are poignant examples. These observations are in very good agreement with the results in ref. [28].

The shapes of the K-factors, however, exhibit some deviations from the results of ref. [28] for the polarisation definition in the laboratory frame. For $|y_{\mathrm{e}^+}| > 2$, the differential K-factor for the LL contribution is increased by up to 7% compared to the literature. A similar deviation can be seen in the differential K-factors for $\cos\theta^*_{\mu^+}$. For $|\cos\theta^*_{\mu^+}| > 0.85$ the K-factor of the LL (TL) contributions decreases from $K \approx 1.8$ (1.6) to values around 1 in the first and last bin, an effect not seen in the literature. A comparison of results at fixed LO with LO+PS predictions reveals that effects are induced by higher-order corrections effected by the parton shower. They raise the cross section for the LL and TL distributions in the phase space regions near θ^* of 0 and π, respectively. The shower in the LO+PS simulation thus already covers parts of the NLO corrections in those phase space regions. Hence, the K-factor, and thus the remaining NLO correction, are decreasing as a consequence. It is interesting to note that a similar effect can be seen for the longitudinal polarisations of the W boson in $\cos\theta^*_{e^+}$. The $\cos\theta^*_{\mu^+}$ distributions for polarisations defined in the COM, however, do not show such a large growth in LO+PS distributions compared to the fixed LO results. This is consistent with the observation that deviations in the K-factors only occur for the Lab decay angles.

JHEP04(2024)001

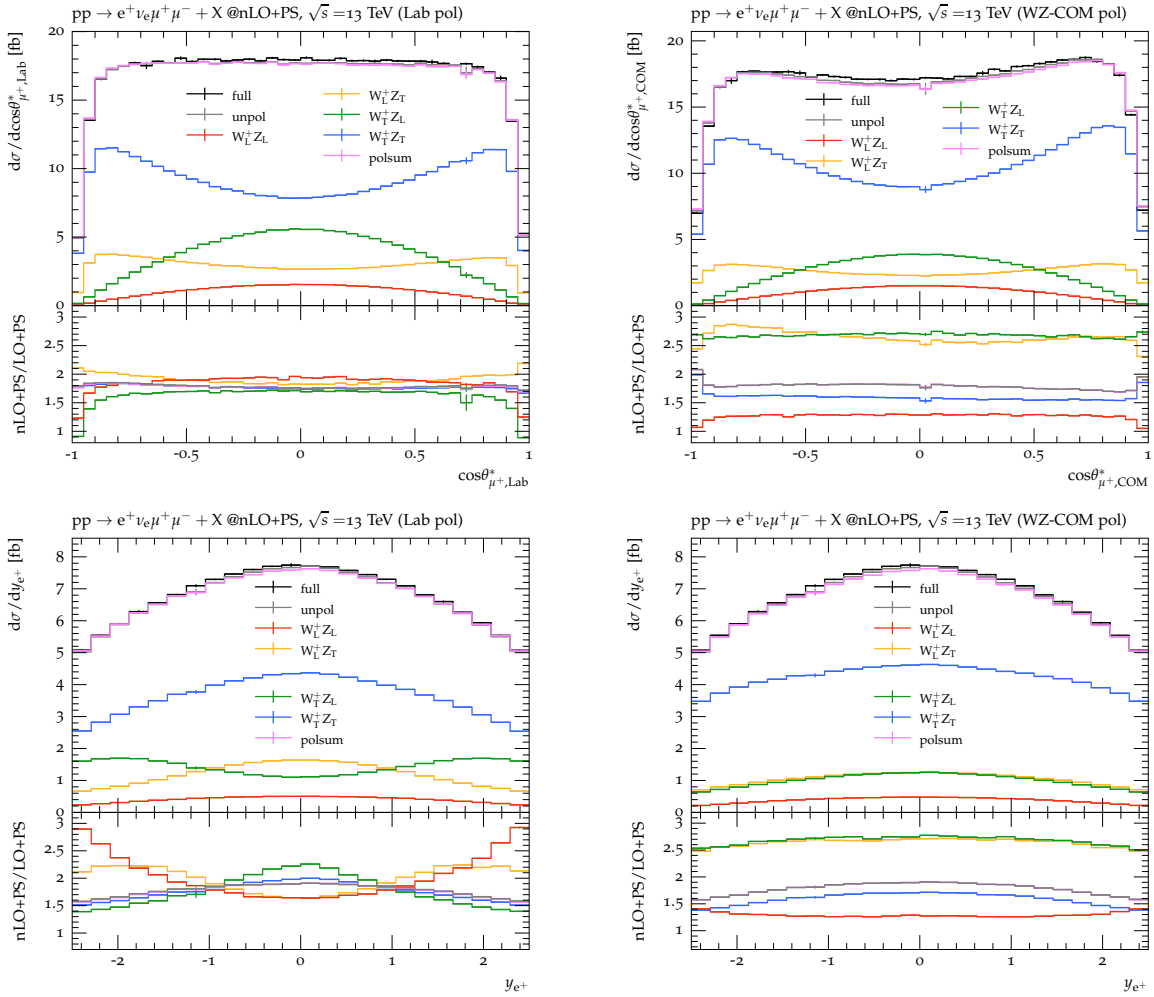

Figure 7. Double-polarised distributions of the anti-muon decay angle $\cos\theta^*_{\mu^+}$ (top) and the positron rapidity y_{e^+} (bottom) in inclusive W^+Z production obtained with SHERPA at nLO+PS (polarised distribution) / NLO+PS (unpol, full) accuracy; polarisation states are defined in the laboratory (Lab, left) and the W^+Z center-of-mass frame (WZ-COM, right), K-factors are the ratio of n(N)LO+PS over LO+PS cross sections. All SHERPA distributions agree well with MOCANLO+COLLIER+RECOLA [25, 26] full NLO fixed-order predictions in ref. [28], figures 1 and 3.

All in all, the SHERPA nLO+PS calculation, despite its reduced formal accuracy, can reproduce the shapes and K-factors of ref. [28] for all investigated observables excellently, with the added benefit of being matched to parton shower evolution and fully differential event simulation.

5.3 Polarised cross sections in multijet-merged calculations

In this section we study the combination of tree-level multijet-merged calculations with the new polarisation framework in SHERPA, again using the example of inclusive W^+Z production. We investigate whether the dependency of the polarised cross sections on the merging scale matches the expectations, i.e.

JHEP04(2024)001

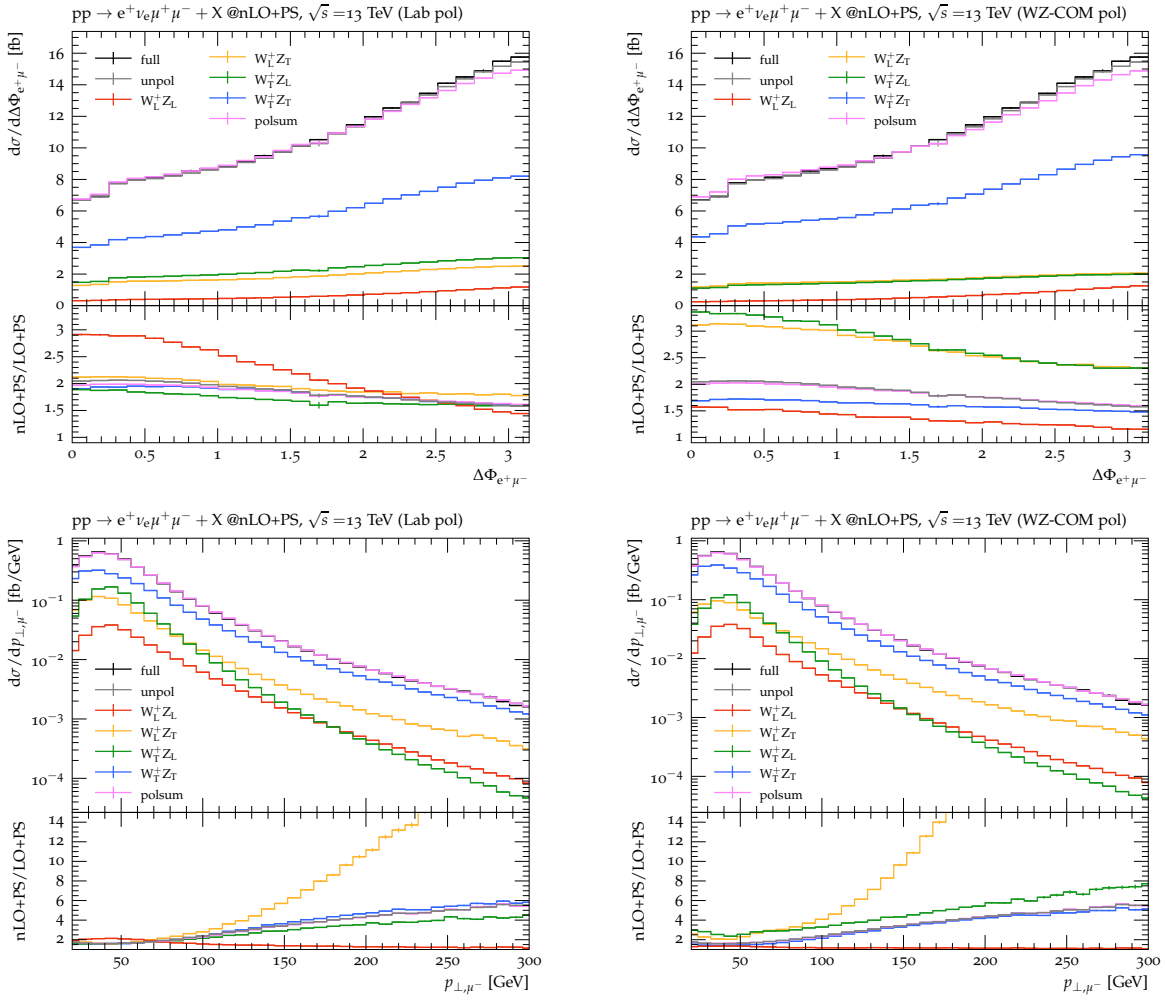

Figure 8. Double-polarised distributions of the azimuthal angle between the positron and the muon $\Delta\Phi_{e^+\mu^-}$ (top) and the muon transverse momentum $p_{\perp,\mu^-}$ (bottom) in inclusive W^+Z production. Details as in figure 7. The $\Delta\Phi_{e^+\mu^-}$ distributions are also calculated with MOCANLO+COLLIER+RECOLA [25, 26] at full NLO fixed-order in ref. [28], figure 5. The SHERPA results shown here agree well with these literature results.

Small merging scales. The resolved (according to the merging scale) one-jet emission corrections to the parton shower are applied over large parts of the phase space, similar to in an NLO-matched calculation. Hence, in cases where the exact virtual correction in an NLO-matched calculation has negligible impact on polarisation correlations, i.e. where our above nLO-matched approximation is valid, we expect to recover very similar polarisation fractions in this case.

Large merging scales. The resolved (according to the merging scale) one-jet emission corrections to the parton shower are applied over only a small fraction of phase space. We thus expect to recover polarisation fractions more and more similar to those at LO.

Table 5 and figure 9 summarise the integrated cross sections and polarisation fractions obtained from these merged calculations (LO+1j) with different merging scales applied and polarisation

JHEP04(2024)001

W^+Z	$\sigma^{\text{nLO+PS}}_{\text{SHERPA}}$ [fb]	K	$\sigma^{Q_c=20\text{GeV}}_{\text{SHERPA}}$ [fb]	K	$\sigma^{Q_c=40\text{GeV}}_{\text{SHERPA}}$ [fb]	K	$\sigma^{Q_c=80\text{GeV}}_{\text{SHERPA}}$ [fb]	K
full	33.95(4)		29.633(28)		29.311(20)			
unpol	33.439(24)	1.78	29.357(10)	1.56	29.124(10)	1.55	27.194(9)	1.45
int	0.235(10)	1.72	0.178(5)	1.31	0.166(4)	1.21	0.117(4)	0.86
L-L	1.891(7)	1.28	1.6656(15)	1.12	1.6686(14)	1.13	1.6095(14)	1.09
L-T	5.231(7)	2.61	4.6227(29)	2.31	4.4568(27)	2.22	3.9203(23)	1.96
T-L	5.007(6)	2.66	4.3994(25)	2.34	4.2086(23)	2.24	3.6560(21)	1.94
T-T	21.074(17)	1.58	18.491(8)	1.39	18.625(7)	1.40	17.890(7)	1.35
	$\sigma^{Q_c=200\text{GeV}}_{\text{SHERPA}}$ [fb]	K	$\sigma^{Q_c=500\text{GeV}}_{\text{SHERPA}}$ [fb]	K	$\sigma^{Q_c=1000\text{GeV}}_{\text{SHERPA}}$ [fb]	K	$\sigma^{\text{LO+PS}}_{\text{SHERPA}}$ [fb]	
unpol	22.221(13)	1.18	19.324(11)	1.03	18.870(11)	1.00	18.803(10)	
int	0.115(6)	0.84	0.121(5)	0.89	0.136(5)	1.00	0.137(4)	
L-L	1.5052(22)	1.02	1.4871(21)	1.00	1.4857(21)	1.00	1.4823(18)	
L-T	2.7834(30)	1.39	2.1168(23)	1.06	2.0122(21)	1.00	2.0041(18)	
T-L	2.5805(27)	1.37	1.9824(21)	1.05	1.8926(20)	1.01	1.8821(17)	
T-T	15.236(10)	1.15	13.616(9)	1.02	13.343(9)	1.00	13.298(8)	

Table 5. Integrated double-polarised cross sections for the simulation of inclusive W^+Z production with up to one jet merged to parton shower at LO. Polarised cross sections and K-factors (K) for different merging scales Q_c are shown in comparison with nLO+PS and LO+PS results. Polarisation states are defined in the W^+Z-center-of-mass frame (COM), K-factors are obtained from dividing the nLO+PS and LO+1j cross sections by the LO+PS cross section, statistical errors on the K-factors are of the order of $\mathcal{O}(10^{-3})$, except for the interference ($\mathcal{O}(10^{-1})$).

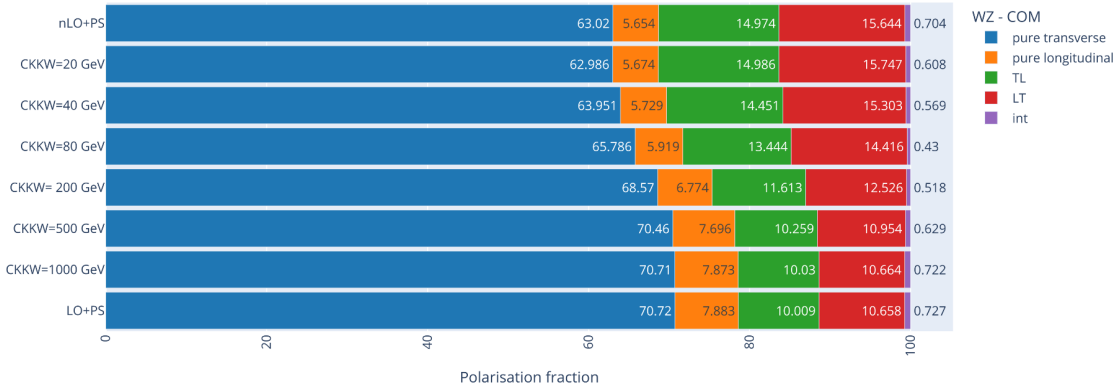

Figure 9. W^+Z center-of-mass frame (COM) polarisation fractions for inclusive W^+Z production at nLO+PS, LO+PS and LO+1j merged with PS with different CKKW-merging scales Q_c between 20 and 1000 GeV. Polarisation fractions are calculated relative to the unpolarised result from data given in table 5.

JHEP04(2024)001

defined in the W^+Z-COM frame. Results for LO+PS and nLO+PS simulations are given for comparison. Comparing the off-shell (full) and unpolarised on-shell (unpol) calculations in the nLO+PS and the multijet-merged setup with the smallest merging scale investigated, a deviation of 15% for the total cross section is mainly caused by the missing virtual corrections in the merged results. All polarised cross sections and associated K factors are reduced accordingly. Conversely, the polarisation fractions when calculated using a reasonably low merging scale of $Q_c = 20\,\text{GeV}$ agree remarkably well with the nLO+PS result at the sub-percent level or better. Hence, the missing finite real-emission corrections to the parton shower for emissions with scales below 20 GeV have no relevant effect on the polarisation fractions, in line with the soft-collinear factorisation of the amplitudes. With increasing merging scale, a continuous change of cross sections, K-factors and polarisation fractions towards the LO results can be observed, reaching it for $Q_c \gtrsim 500\,\text{GeV}$. It is interesting to note that not all polarisation fractions are equally affected by the absence (or presence) of hard-emission corrections in the different multijet-merged calculations. While, e.g., the fraction of the cross section carried by the interference of different polarisation states is reduced by 7% when raising Q_c from 20 to 40 GeV, the fraction of the cross section wherein both VBs are polarised longitudinally remains approximately constant. In summary, the use of merging scales $Q_c > 40\,\text{GeV}$ is counter-indicated if real-emission effects are considered to be important to accurately describe the polarisation fractions in a given sample. We will thus restrict our discussion in the remainder of this section to reasonable merging scales $Q_c \leq 40\,\text{GeV}$.

We now turn to examine differential distributions. Figure 10 displays the polarised distributions in the muon transverse momentum, $p_{\perp,\mu^-}$, and the azimuthal separation between positron and muon, $\Delta\Phi_{e^+\mu^-}$, obtained at nLO+PS and from tree-level merged calculations with reasonably small merging scales (20 and 40 GeV) to illustrate the influence of merged calculations on distributions w.r.t. the nLO+PS result (upper ratio plot) and the effect of a merging scale variation (lower ratio plot). The ratios of the polarised contributions are calculated with respect to their counterparts in the nLO+PS/$Q_c = 20\,\text{GeV}$ simulations.

The missing virtual and exact real-emissions corrections for very soft-collinear emission at scales below 20 GeV reduce all merged distributions by roughly 15% w.r.t. the nLO+PS results,[7] as already observed for the integrated results. Their influence is, however, not constant over the entire investigated phase space. This can be seen in particular for the muon transverse momentum $p_{\perp,\mu^-}$. Similarly, the impact of the missing virtual and very soft-collinear real-emission corrections also depends on the polarisation state under consideration and the frame they are defined in. In particular, the LL component reveals a markedly different behaviour compared to all other polarisation combinations. Not only does this polarisation combination exhibit a smaller impact of these missing contributions w.r.t. the nLO+PS result at large $p_{\perp,\mu^-}$, $\Delta\Phi_{e^+\mu^-}$, it also shows a frame dependent effect of these contributions at small lepton azimuthal separations $\Delta\Phi_{e^+\mu^-}$. In either case, though, all mismodeling effects w.r.t the nLO+PS result are contained within $\approx 5\%$ of the flat K-factor hypothesis for the dominant polarisation combination and only reach a deviation of up to 10% (20%) for $\Delta\Phi_{e^+\mu^-}$ ($p_{\perp,\mu^-}$) for the strongly suppressed LL contribution.

As a consequence of the above observations, the merging scale variation (lower ratio plot in figure 10), varying the amount of exact real-emission corrections effected onto the

[7] We remind the reader that our nLO+PS results are in fact NLO accurate for unpolarised observables.

JHEP04(2024)001

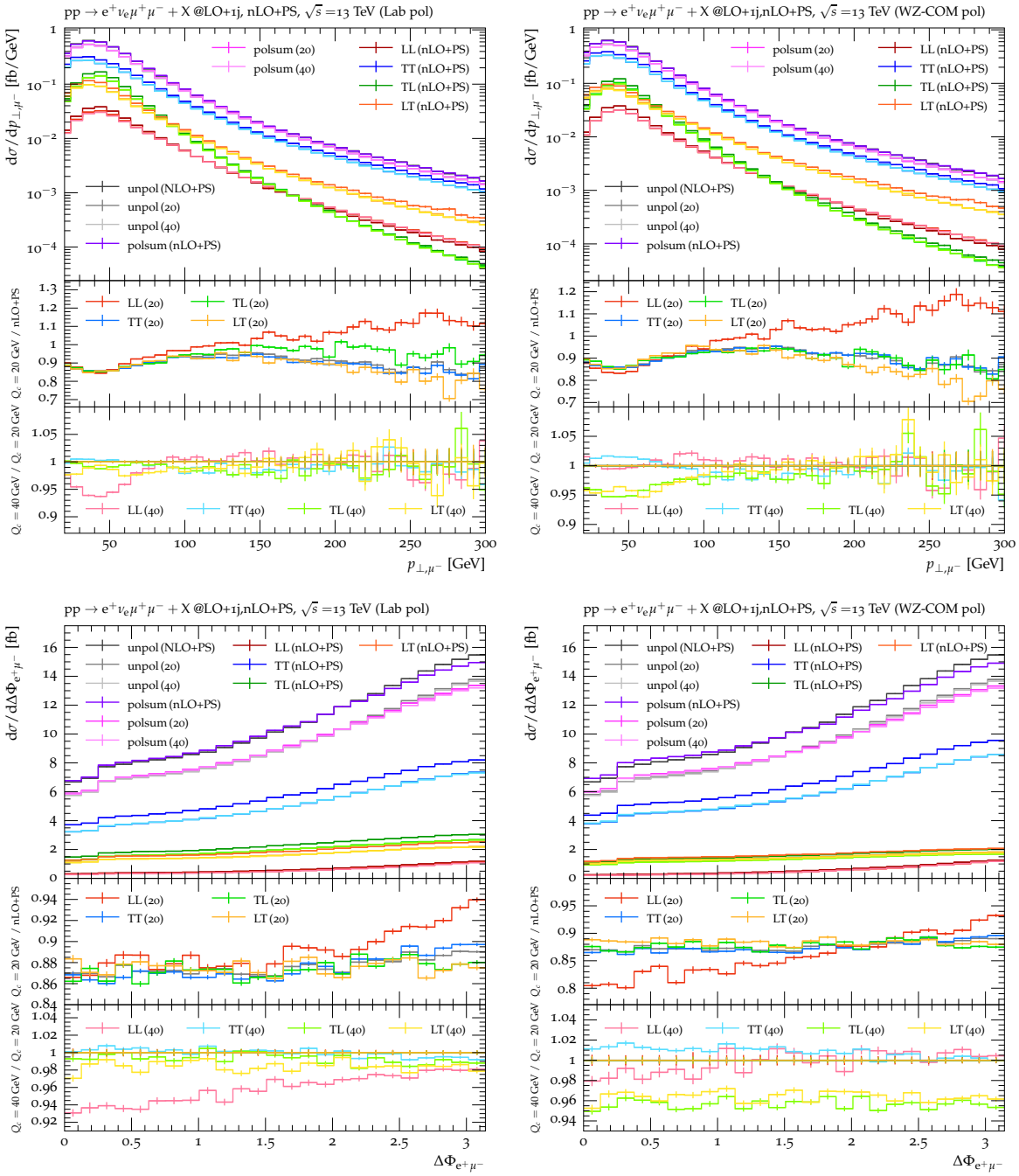

Figure 10. Double-polarised distributions of the muon transverse momentum $p_{\perp,\mu^-}$ (top) and the azimuthal separation of the positron and the muon $\Delta\Phi_{e^+\mu^-}$ (bottom) for the inclusive W^+Z-production process. SHERPA results obtained with LO+1j merged calculations with CKKW-merging scales of 20 and 40 GeV are shown in comparison with results at nLO+PS accuracy. Polarisation states are defined in the laboratory frame (left) and the W^+Z-center-of-mass frame (right). Legend entries in each of the subpanels are valid for the whole subfigure. For the $p_{\perp,\mu^-}$ distributions, the polsum results superimpose the corresponding unpol cross sections almost perfectly, which is why the latter are barely visible in the main panel.

JHEP04(2024)001

parton shower, also affects different polarisation states and definitions differently. For the polarisation states defined in the laboratory frame, the missing real-emission corrections from the one-jet matrix element between 20 and 40 GeV only have a significant influence on the LL component, again, for $\Delta\Phi_{e^+\mu^-} < 2.5$ and $p_{\perp,\mu^-} < 80\,\text{GeV}$, while, conversely, for the COM definition they only have a noticeable impact on mixed polarised cross sections (LT and TL) in the whole $\Delta\Phi_{e^+\mu^-}$ phase space and for $p_{\perp,\mu^-} < 100\,\text{GeV}$. For these polarisation combinations an accurate description of emissions at moderate scales, $20 - 40\,\text{GeV}$, is vital. The TT polarisation combinations in both the Lab and COM frame definitions, however, remain nearly unaffected by the merging scale variation with deviations of 2% or less.

Connecting these merging scale dependences with the K-factor dependence of the different polarisation states we find some correlation between the two. In phase space regions where polarisation states are affected by the merging scale variation they also exhibit the largest nLO corrections (see K-factors in figure 8) compared to the other polarisation components. Thus, emissions between 20 and 40 GeV are at least partly responsible for these increased K-factors. The shape of the increased TL and LT K-factors for $\Delta\Phi_{e^+\mu^-}$ in the COM polarisation definition as well as the giant TL and LT K-factors for large $p_{\perp,\mu^-}$ observed for both investigated polarisation definitions, however, can not be explained by contributions from emissions below 40 GeV. Here, hard emission corrections, beyond scales of 40 GeV, contained in both nLO+PS and this multijet-merged calculation, seem to play the dominant role.

6 Conclusions

In this paper we presented a new implementation enabling the MC event generator Sherpa to simulate polarised cross sections for an arbitrary number of intermediate vector bosons. The simulation itself remains unpolarised, comprising all polarisation components. However, the individual polarised cross sections are made available as additional event weights such that polarised cross sections for all possible polarisation combinations as well as all interferences between different polarisation states, which are made available here for the first time, can be calculated in a single simulation run. All common reference systems are supported, and new frames of interest can easily be implemented.

We validated our implementation at fixed LO revealing excellent agreement with the literature despite using different approximations to define the on-shell intermediate vector bosons (we use the narrow-width approximation, whereas the double-pole approximation was used in the reference results). Using the example of inclusive W^+Z production, we have shown that our framework is not only able to calculate polarised cross sections at LO accuracy, but can also incorporate NLO corrections by using the new polarisation framework together with Sherpa's Mc@Nlo matching. In this way, we have presented the first nLO+PS matched predictions for polarised cross sections, showing important improvements over their only LO accurate counterparts available up until now.

Further, we have presented the combination of our new polarisation framework with Sherpa's multijet-merging calculations, making polarised multijet calculations available. We have shown that, similarly to the unpolarised case, most features of the nLO accurate polarisation fractions, apart from a global normalisation factor, can be reproduced. The additional systematics typically associated with this approach are negligible for integrated

JHEP04(2024)001

polarisation fractions, but can start to play a role for some subleading polarisation components in typical observables.

In the future, we plan to extend our polarisation framework to full NLO accuracy in the vector boson production part by including the complete virtual contributions in the calculation of the amplitude tensor. With that, we will also be able to include approximate NLO EW corrections in the EW_{virt} [46] scheme in the simulation of polarised cross sections with Sherpa. A simulation of polarised cross sections with full NLO accuracy throughout requires the inclusion of higher order contributions in the decay part of the processes, which is more challenging and will follow in a second step.

Acknowledgments

The authors would like to thank Giovanni Pelliccioli for helpful discussions about Phantom and the definition of polarised cross sections in general as well as Stefan Höche for his help with the polarisation definition in Sherpa's build-in matrix element generator Comix. After the submission of this work, a related manuscript appeared in ref. [59], providing a nice comparison to our approach and results.

M.S. is supported by the U.K. Science and Technology Facilities Council (STFC) Consolidated Grant programme ST/T001011/1 and by the Royal Society through a University Research Fellowship (URF\R1\180549, URF\R\231031) and Enhancement Awards (RGF\EA\181033, CEC19\100349, and RF\ERE\210397). This work has received funding from the European Union's Horizon 2020 research and innovation programme as part of the Marie Skłodowska-Curie Innovative Training Network MCnetITN3 (grant agreement no. 722104).

A Simulation of polarised cross sections with Sherpa

A.1 Input structure for calculating polarised cross sections with Sherpa

In this section, the structure of the run card parts relevant for simulating polarised cross sections with Sherpa is discussed. In order to allow for the calculation of polarised cross sections, `Hard_Decays` need to be enabled. Gauge invariance is retained by setting the VB widths to zero. This leads to real couplings.

The simulation of polarised cross sections in Sherpa itself is steered by an own block called `Pol_Cross_Section` within the `Hard_Decays` scoped setting in the Sherpa run card. The following settings are possible:

`Enabled:` `<true/false>` enables the calculation of polarised cross sections on top of the simulation of unstable intermediate particles.

`Spin_Basis` specifies the spin basis. Beside the helicity basis (`Helicity`, default), constant reference vectors a^μ are supported, e.g. `1.0, 0.0, 0.0, 0.0`, which define the spin axis as shown in eq. (2.6). Per simulation, only one spin basis can be used.

`Reference_System` denotes the reference system used for polarisation definition. Currently, the laboratory system (`Lab`, default), the center-of-mass frame of all intermediate particles

JHEP04(2024)001

(`COM`), the parton-parton-frame (`PPFr`) and the rest frames defined by any combination of the initial or final state particles in the VB production process are supported. The first three systems are specified by the corresponding keywords, for the latter the particle numbers (according to Sherpa's internal particle numbering) of the particles defining the rest frame need to be given, separated by white spaces, e.g. `2 3`. In one simulation run, more than one reference system can be considered by passing a list of desired reference systems here.

`Transverse_Weights_Mode` allows to switch between the coherent (mode `1`, default) and the incoherent (mode `0`) definition of transverse polarisation states (see appendix A.2 for details), also weights for both definitions can be calculated at the same time (mode `2`).

`Weight<`*n*`>` can be used to specify weights which should be calculated additionally to the base polarisation weights which are output during each simulation run, see appendix A.2 for details. `<`*n*`>` needs to be replaced by an integer. By using different integers, more than one custom weight can be calculated.

With that, the parts of the run card relevant for the simulation of polarised cross sections e.g. in section 5 are:

```
WIDTH_SCHEME: Fixed  # real couplings

# Gauge of the Weyl spinors to receive the representation of the
# polarisation vectors in eq. (2.4)
COMIX_DEFAULT_GAUGE: 0

PARTICLE_DATA:
  24: {Width: 0}
  23: {Width: 0}

HARD_DECAYS:
  Enabled: true
  Pol_Cross_Section:
    Enabled: true
    Spin_Basis: Helicity    # default
    Reference_System: [Lab, COM]
    Transverse_Weights_Mode: 1  # default
    Weight1: 2
    Weight2: 3
```

A.2 Output structure: provided polarisation weights

As introduced in section 3, polarised cross sections of all possible polarisation combinations of the intermediate particles are provided as additional event weights in Sherpa. There are three different categories of polarisation weights in Sherpa:

Base polarisation weights are output during each simulation of polarised cross sections and include all contributions where all intermediate VBs are in a defined polarisation state

JHEP04(2024)001

(for VBs: left(-)-handed, right(+)-handed or longitudinal (0) polarisation mode). Corresponding weight names have the form `PolWeight_<Referencesystem>.particle1.`λ_1`_particle2.`$\lambda_2\ldots$ with $\lambda_i \in \{+,-,0\}$. The order of the particles in the weight names is determined by SHERPA's internal particle ordering. Furthermore, all interference terms are totalled to an overall interference contribution with the label `PolWeight_<Referencesystem>.int`.

Transversely polarised weights describing contributions of polarisation combinations where at least one massive VB is transversely polarised are also output per default. Two distinct definitions for the transverse polarisation are supported:

- **incoherent definition:** left- and right-handed polarised contributions are added to a transverse contribution. Corresponding weights contain a small **"t"** for each transverse polarised particle, e.g. `PolWeight_Lab.W+.t`.
- **coherent definition:** besides the left- and right-handed polarised contributions also left-right-interference terms are included in the definition of the transverse contribution. This definition is more common in the literature [27–29, 37, 41, 47] and is also used by other generators, e.g. MADGRAPH. Thus, it is also the default choice in SHERPA. If this definition is chosen, also an adjusted interference weight is calculated with the weight name `PolWeight_<Referencesystem>.coint`. Corresponding weights are recognizable by a capital **"T"** for each transverse polarised particle, e.g. `PolWeight_Lab.W+.T`.

Custom polarisation weights are only calculated if specified in the SHERPA run card. The corresponding setting is `Weight<`n`>` where n is an integer such that it is possible to request more than one custom weight. Depending on the type of custom weights either weight names or particle numbers used to specify which weight should be calculated additionally. The following custom weights can be provided by SHERPA:

- **partially unpolarised weights:** Intermediate particles, that shall be considered as unpolarised, can be specified by a comma-separated list of their particle numbers according to SHERPA's internal particle numbering in the run card. The associated weight names have the form `PolWeight_<Referencesystem>.Weight<`n`>_particle1.U_particle2.U..._particlei.`$\lambda_i\ldots$ where particles $1-(i-1)$ are considered as unpolarised. `Weight<`n`>` corresponds to the setting name in the SHERPA run card to distinguish between different sets of unpolarised particles. The ordering of the unpolarised and the polarised particles among itself is again according to SHERPA's internal particle ordering. In addition, a new interference weight is calculated (`PolWeight_<Referencesystem>.Weight<`n`>_particle1.U_particle2.U..._int`). It contains less terms than the interference corresponding to the base weights, since the polarisation weights in which the remaining polarised intermediate particles have a definite polarisation also contain interference terms from the now unpolarised particle. For example, if a process with two VBs is considered and the VB with the polarisation indices λ_1, λ_1' in eq. (3.1) remains unpolarised then the following entries of the amplitude tensor would contribute to the resulting single-polarised (=one of two intermediate VBs is in a definite polarisation state) longitudinal weight with the

JHEP04(2024)001

interference terms in square brackets:

$$|\mathcal{M}_{\text{singlepol}}|^2_{00} = |\mathcal{M}|^2_{+0+0} + |\mathcal{M}|^2_{-0-0} + |\mathcal{M}|^2_{0000} + \Big[|\mathcal{M}|^2_{+0-0} + |\mathcal{M}|^2_{+000} + |\mathcal{M}|^2_{-0+0} + |\mathcal{M}|^2_{-000} + |\mathcal{M}|^2_{00+0} + |\mathcal{M}|^2_{00-0}\Big].$$

- **individual interference weights:** Interference weight names have two instead of one polarisation index per particle (first index stands for the polarisation of the particle in the corresponding matrix element, the second index for its polarisation in the complex conjugate matrix element). If provided within the `Weight<n>` setting, the corresponding interference weight is output and labelled by its weight name.
- **sum of specified weights:** All weights from those mentioned beforehand, which are specified as comma separated list of their weight names in the run card, are totalled and labelled as `PolWeight_<Referencesystem>.Weight<n>` where `Weight<n>` is again the corresponding setting in the Sherpa run card.

B Validation setups and further results

This appendix summarises the simulation setups used for the validation study presented in section 4 in section B.1. Furthermore, some additional validation results are given in section B.2.

B.1 Validation setups

In order to reproduce the results from the literature studies in ref.s [37, 41, 47], the simulation parameters and phase space definitions given in tables 6 and 7, respectively are chosen identical to the literature. Polarised cross sections with and without applying lepton acceptance criteria are investigated and denoted as **"fiducial"** and **"inclusive"** setup, respectively. All fermions except the top quark are considered as massless, if not stated otherwise. A b-veto is understood as a perfect b-veto on initial and final states. The cross sections studied, whether single- or double-polarised, and the definitions of polarisation investigated, match those found in the literature.

Rivet analyses used to analyse the simulation data are based on the ATLAS analysis of ref. [61] (ZZjj), on the Rivet analyses of ref. [62] (W^+W^+jj) and ref. [63] (W^+Zjj validation against ref. [41]) or on private Rivet analyses (W^+Zjj validation against ref. [47], W^+W^-jj). The study of the W^+Zjj process in ref. [41] uses a dedicated procedure to reconstruct neutrinos for the calculation of $W^\pm$ boson observables which is taken into account in the associated Rivet analysis. For all other process, perfect neutrino reconstruction is assumed. Within the event generation, only selection criteria on final state particles of the hard scattering process (= VB production subprocess) can be applied. All remaining selection criteria are then implemented in the subsequent Rivet-analysis.

For all processes, observables are investigated that can only be defined for the mixed lepton flavour decay channel of the VB pair if the VBs are identical. Same flavour lepton decay channels which can not be excluded by Sherpa during the simulation of several identical

JHEP04(2024)001

PDF-Set from LHAPDF6 [57]	NNPDF30_lo_as_0130 [60]
Electroweak scheme	G_μ scheme with $G_\mu = 1.16637 \cdot 10^{-5}$ GeV^{-2}
	and $\alpha_{\text{EW}} = \frac{\sqrt{2} G_\mu M_{\text{W}}^2}{\pi} \left(1 - \left(\frac{M_{\text{W}}}{M_{\text{Z}}}\right)^2\right)$
	complex mass scheme (full),
	real EW parameters (polarisation) [37]
Strong coupling $\alpha_S(M_Z^2)$	0.130
Factorisation scale	[37, 41]: $\mu_F = M_{4\text{l}}/\sqrt{2}$, [47]: $\mu_F = \sqrt{p_{\perp,\text{j}_1} p_{\perp,\text{j}_2}}$
VB pole masses	$M_{\text{W}} = 80.358$ GeV, $M_{\text{Z}} = 91.153$ GeV
VB pole widths	zero for all VBs in polarisation calculations,
	$\Gamma_{\text{W}} = 2.084$ GeV, $\Gamma_{\text{Z}} = 2.494$ GeV otherwise

Table 6. Simulation settings used for SHERPA simulations within the validation study of the new SHERPA polarisation framework against literature data.

General selection requirements	
inclusive phase space	fiducial phase space
$\lvert\eta_{\text{j}}\rvert < 5$	cf. inclusive phase space
$p_{\perp,\text{j}} > 20\,\text{GeV}$	$\lvert\eta_{\text{l}}\rvert < 2.5$
$M_{\text{jj}} > 500\,\text{GeV}$	$p_{\perp,\text{l}} > 20\,\text{GeV}$
$\lvert\Delta\eta_{\text{jj}}\rvert > 2.5$	W^+Vjj: $p_{\perp,\text{miss}} > 40\,\text{GeV}$
Process specific selection requirements	
process (reference)	selection criteria
$\text{W}^+\text{W}^+\text{jj}$ [47]: $\text{pp} \to \text{e}^+ \nu_e \mu^+ \nu_\mu \text{jj}$	$M_{4l} > 161\,\text{GeV}$ [8]
$\text{W}^+\text{W}^-\text{jj}$ [47]: $\text{pp} \to \text{e}^+ \nu_\text{e} \mu^- \bar{\nu}_\mu \text{jj}$	b-veto, $M_{4\text{l}} > 2M_{\text{W}}$
$\text{W}^+\text{W}^-\text{jj}$ [37]: $\text{pp} \to \mu^+ \nu_\mu \text{e}^- \bar{\nu}_\text{e} \text{jj}$	b-veto, $M_{4\text{l}} > 300\,\text{GeV}$, lepton selection criteria only on e^-
	$M_{\text{jj}} > 600\,\text{GeV}$, $\lvert\Delta\eta_{\text{jj}}\rvert > 3.6$, $\eta_{\text{j}_1} \cdot \eta_{\text{j}_2} < 0$
W^+Zjj [47]: $\text{pp} \to \text{e}^+ \nu_\text{e} \mu^+ \mu^- \text{jj}$	b-veto, $M_{4\text{l}} > 200\,\text{GeV}$, $\lvert M_{\text{e}^+\text{e}^-} - M_{\text{Z}}\rvert < 10\,\text{GeV}$
W^+Zjj [41]: $\text{pp} \to \mu^+ \nu_\mu \text{e}^+ \text{e}^- \text{jj}$	b-veto, $M_{4\text{l}} > 200\,\text{GeV}$, $\lvert M_{\text{e}^+\text{e}^-} - M_{\text{Z}}\rvert < 15\,\text{GeV}$
ZZjj [47]: $\text{pp} \to \text{e}^+ \text{e}^- \mu^+ \mu^- \text{jj}$	b-veto, $M_{4\text{l}} > 200\,\text{GeV}$, $\lvert M_{\text{l}^+\text{l}^-} - M_{\text{Z}}\rvert < 10\,\text{GeV}$
ZZjj [41]: $\text{pp} \to \text{e}^+ \text{e}^- \mu^+ \mu^- \text{jj}$	b-veto, $M_{4\text{l}} > 200\,\text{GeV}$, $\lvert M_{\text{l}^+\text{l}^-} - M_{\text{Z}}\rvert < 15\,\text{GeV}$

Table 7. Selection criteria used for SHERPA simulations within the validation study of the new SHERPA polarisation framework against literature data.

VBs (ZZjj, $\text{W}^+\text{W}^+\text{jj}$ process), are then vetoed during the RIVET-analyses for all observables. Therefore, no ambiguity for the reconstruction of the VBs from their decay products exist. Corresponding single-polarised cross sections are calculated by a private extension of the

[8] The M_{4l} selection requirement for the $\text{W}^+\text{W}^+\text{jj}$ process is only applied during the polarisation calculation.

JHEP04(2024)001

ZZjj	σ_{PHANTOM} [fb]	Fraction [%]	σ_{SHERPA} [fb]	Fraction [%]
full	0.06102(4)		0.060987(27)	
unpol	0.06059(4)	100	0.06116(4)	100
polsum	0.05891(2)	97.23(7)	0.059452(29)	97.21(8)
int	0.00168(4) (diff)	2.77(7)	0.001712(24)	2.80(4)
long-unpol	0.01619(1)	26.721(24)	0.016230(15)	26.536(29)
left(-)-unpol	0.02676(2)	44.17(4)	0.027079(21)	44.27(4)
right(+)-unpol	0.01595(1)	26.324(24)	0.016143(14)	26.394(28)

Table 8. Integrated single-polarised cross sections for the ZZjj process at fixed LO obtained with PHANTOM in ref. [41] and SHERPA in the fiducial phase space introduced in section B.1; single-polarised cross sections are given for the Z boson decaying into an electron-positron pair being polarised; the polarisation is defined in the laboratory frame; polarisation fractions are calculated relative to the unpolarised result.

presented polarisation framework, where all polarisation combinations are totalled, leaving only the VB decaying via a specified decay channel polarised. The resulting weights are set to zero for same flavour decay channels.

B.2 Integrated polarised cross sections in the presence of lepton acceptance requirements

This appendix presents integrated cross sections computed in the fiducial phase spaces defined in section B.1 to supplement the distributions discussed in section 4. Resulting integrated cross sections are displayed in tables 8–10. Interference predictions from the literature are calculated as difference between the unpolarised result (unpol) and the sum of all polarised contributions (polsum) for comparison.

For all four processes, the unpolarised result reproduces the full cross section at the 1% level, indicating small non-resonant contributions and low off-shell effects not covered by the mass smearing. For the W^+W^-jj process, it was not possible to achieve a perfect agreement of the full results from SHERPA and PHANTOM. However, since the literature only provides polarisation fractions (relative to the full!) for this process, this does not pose a limitation for the comparison.

If given, polarised cross sections, polarisation and interference fractions obtained with SHERPA are in very good agreement with the literature for all processes showing deviations of 1.5% or less.

JHEP04(2024)001

W^+W^-jj	σ_{PHANTOM} [fb]	Fraction [%]	σ_{SHERPA} [fb]	Fraction [%]
full	1.411(1)	100	1.3537(11)	100
unpol	1.401(1)	99.29(10)	1.3497(5)	99.70(9)
polsum	1.382(1)	97.94(10)	1.3309(9)	98.32(11)
int	0.019(1) (diff)	1.35(7)	0.0188(8)	1.39(6)
long		21	0.28969(33)	21.400(30)
left(-)		52	0.7047(5)	52.06(6)
right(+)		25	0.3365(4)	24.86(4)

Table 9. Integrated cross sections for the W^+W^-jj process at fixed LO obtained with PHANTOM in ref. [37] and SHERPA in the fiducial phase space introduced in section B.1; single-polarised cross sections are given for the W^- boson being polarised; the polarisation is defined in the laboratory frame; polarisation fractions are calculated relative to the full result.

W^+Zjj	σ_{PHANTOM} [fb]	Fraction [%]	σ_{SHERPA} [fb]	Fraction [%]
full	0.1651(1)		0.16519(5)	
unpol	0.1642(2)	100	0.16342(9)	100
Z boson polarised				
int	0.0040(2) (diff)	2.43(12)	0.00397(7)	2.43(4)
right(+)	0.04054(3)	24.689(35)	0.04042(4)	24.734(28)
left(-)	0.07687(6)	46.81(7)	0.07657(5)	46.86(4)
long	0.04256(3)	25.920(36)	0.04246(4)	25.980(27)
W^+ boson polarised				
int	0.0038(2) (diff)	2.31(12)	0.00362(7)	2.22(5)
right(+)	0.03093(2)	18.837(26)	0.03085(4)	18.880(26)
left(-)	0.09631(8)	58.65(9)	0.09602(7)	58.75(5)
long	0.03321(3)	20.225(31)	0.03293(4)	20.148(25)

Table 10. Integrated single-polarised cross sections for the W^+Zjj process at fixed LO obtained with PHANTOM in ref. [41] and SHERPA in the fiducial phase space introduced in section B.1; the polarisation is defined in the laboratory frame; polarisation fractions are calculated relative to the unpolarised result.

JHEP04(2024)001

W^+W^+jj	σ_{PHANTOM} [fb]	Fraction [%]	σ_{SHERPA} [fb]	Fraction [%]
full	1.593(2)		1.5901(13)	
unpol	1.572(2)	100	1.5728(8)	100
		Laboratory frame		
int (single)	-0.0156(23) (diff)	-0.99(15)	-0.0141(4)	-0.898(26)
T-unpol	1.165(1)	74.11(11)	1.1646(6)	74.05(5)
L-unpol	0.4226(4)	26.88(4)	0.4223(4)	26.851(27)
int (double)	-0.0279(22) (diff)	-1.77(14)	-0.0281(7)	-1.78(4)
L-L	0.1185(1)	7.538(12)	0.11837(19)	7.526(13)
TL+LT	0.6124(6)	38.96(6)	0.6134(5)	39.00(4)
T-T	0.8690(9)	55.28(9)	0.8691(6)	55.26(5)
		W^+W^+-center-of-mass frame		
int (single)	-0.0136(29) (diff)	-0.87(18)	-0.0118(4)	-0.749(26)
T-unpol	1.182(2)	75.19(16)	1.1807(7)	75.07(6)
L-unpol	0.4036(5)	25.67(5)	0.40393(34)	25.682(25)
int (double)	-0.0220(22) (diff)	-1.40(14)	-0.0213(6)	-1.35(4)
L-L	0.1552(2)	9.873(18)	0.15593(21)	9.914(14)
TL+LT	0.5038(6)	32.05(6)	0.5046(4)	32.084(31)
T-T	0.9350(9)	59.48(9)	0.9338(6)	59.37(5)

Table 11. Integrated single- and double-polarised cross sections for the W^+W^+jj process at fixed LO obtained with PHANTOM in ref. [47] and SHERPA in the fiducial phase space introduced in section B.1; single-polarised cross sections are given for the W^+ boson decaying into $e^+\nu_e$ being polarised; the polarisation is defined in the laboratory and the W^+W^+-center-of-mass frame; polarisation fractions are calculated relative to the unpolarised result.

References

[1] D. Espriu and B. Yencho, *Longitudinal WW scattering in light of the "Higgs boson" discovery*, *Phys. Rev. D* **87** (2013) 055017 [arXiv:1212.4158] [INSPIRE].

[2] J. Chang, K. Cheung, C.-T. Lu and T.-C. Yuan, *WW scattering in the era of post-Higgs-boson discovery*, *Phys. Rev. D* **87** (2013) 093005 [arXiv:1303.6335] [INSPIRE].

[3] S. Brass et al., *Transversal Modes and Higgs Bosons in Electroweak Vector-Boson Scattering at the LHC*, *Eur. Phys. J. C* **78** (2018) 931 [arXiv:1807.02512] [INSPIRE].

[4] CMS collaboration, *Measurement of the Polarization of W Bosons with Large Transverse Momenta in W+Jets Events at the LHC*, *Phys. Rev. Lett.* **107** (2011) 021802 [arXiv:1104.3829] [INSPIRE].

JHEP04(2024)001

[5] ATLAS collaboration, *Measurement of the polarisation of W bosons produced with large transverse momentum in pp collisions at $\sqrt{s} = 7$ TeV with the ATLAS experiment*, *Eur. Phys. J. C* **72** (2012) 2001 [arXiv:1203.2165] [INSPIRE].

[6] CMS collaboration, *Measurements of the W boson rapidity, helicity, double-differential cross sections, and charge asymmetry in pp collisions at $\sqrt{s} = 13$ TeV*, *Phys. Rev. D* **102** (2020) 092012 [arXiv:2008.04174] [INSPIRE].

[7] CMS collaboration, *Angular coefficients of Z bosons produced in pp collisions at $\sqrt{s} = 8$ TeV and decaying to $\mu^+\mu^-$ as a function of transverse momentum and rapidity*, *Phys. Lett. B* **750** (2015) 154 [arXiv:1504.03512] [INSPIRE].

[8] ATLAS collaboration, *Measurement of the angular coefficients in Z-boson events using electron and muon pairs from data taken at $\sqrt{s} = 8$ TeV with the ATLAS detector*, *JHEP* **08** (2016) 159 [arXiv:1606.00689] [INSPIRE].

[9] ATLAS collaboration, *Measurement of the W boson polarisation in $t\bar{t}$ events from pp collisions at $\sqrt{s} = 8$ TeV in the lepton + jets channel with ATLAS*, *Eur. Phys. J. C* **77** (2017) 264 [*Erratum ibid.* **79** (2019) 19] [arXiv:1612.02577] [INSPIRE].

[10] CMS collaboration, *Measurement of the W boson helicity fractions in the decays of top quark pairs to lepton + jets final states produced in pp collisions at $\sqrt{s} = 8$ TeV*, *Phys. Lett. B* **762** (2016) 512 [arXiv:1605.09047] [INSPIRE].

[11] CMS and ATLAS collaborations, *Combination of the W boson polarization measurements in top quark decays using ATLAS and CMS data at $\sqrt{s} = 8$ TeV*, *JHEP* **08** (2020) 051 [arXiv:2005.03799] [INSPIRE].

[12] ATLAS collaboration, *Measurement of $W^{\pm}Z$ production cross sections and gauge boson polarisation in pp collisions at $\sqrt{s} = 13$ TeV with the ATLAS detector*, *Eur. Phys. J. C* **79** (2019) 535 [arXiv:1902.05759] [INSPIRE].

[13] CMS collaboration, *Measurement of the inclusive and differential WZ production cross sections, polarization angles, and triple gauge couplings in pp collisions at $\sqrt{s} = 13$ TeV*, *JHEP* **07** (2022) 032 [arXiv:2110.11231] [INSPIRE].

[14] ATLAS collaboration, *Observation of gauge boson joint-polarisation states in W±Z production from pp collisions at $\sqrt{s} = 13$ TeV with the ATLAS detector*, *Phys. Lett. B* **843** (2023) 137895 [arXiv:2211.09435] [INSPIRE].

[15] CMS collaboration, *Measurements of production cross sections of polarized same-sign W boson pairs in association with two jets in proton-proton collisions at $\sqrt{s} = 13$ TeV*, *Phys. Lett. B* **812** (2021) 136018 [arXiv:2009.09429] [INSPIRE].

[16] P. Azzi et al., *Report from Working Group 1: Standard Model Physics at the HL-LHC and HE-LHC*, *CERN Yellow Rep. Monogr.* **7** (2019) 1 [arXiv:1902.04070] [INSPIRE].

[17] CMS collaboration, *Vector Boson Scattering prospective studies in the ZZ fully leptonic decay channel for the High-Luminosity and High-Energy LHC upgrades*, CMS-PAS-FTR-18-014, CERN, Geneva (2018).

[18] J. Alwall et al., *The automated computation of tree-level and next-to-leading order differential cross sections, and their matching to parton shower simulations*, *JHEP* **07** (2014) 079 [arXiv:1405.0301] [INSPIRE].

[19] D. Buarque Franzosi, O. Mattelaer, R. Ruiz and S. Shil, *Automated predictions from polarized matrix elements*, *JHEP* **04** (2020) 082 [arXiv:1912.01725] [INSPIRE].

JHEP04(2024)001

[20] C. Bierlich et al., *A comprehensive guide to the physics and usage of PYTHIA 8.3*, *SciPost Phys. Codeb.* **2022** (2022) 8 [arXiv:2203.11601] [INSPIRE].

[21] M. Bahr et al., *Herwig++ Physics and Manual*, *Eur. Phys. J. C* **58** (2008) 639 [arXiv:0803.0883] [INSPIRE].

[22] J. Bellm et al., *Herwig 7.0/Herwig++ 3.0 release note*, *Eur. Phys. J. C* **76** (2016) 196 [arXiv:1512.01178] [INSPIRE].

[23] A. Ballestrero et al., *PHANTOM: A Monte Carlo event generator for six parton final states at high energy colliders*, *Comput. Phys. Commun.* **180** (2009) 401 [arXiv:0801.3359] [INSPIRE].

[24] S. Actis et al., *Recursive generation of one-loop amplitudes in the Standard Model*, *JHEP* **04** (2013) 037 [arXiv:1211.6316] [INSPIRE].

[25] S. Actis et al., *RECOLA: REcursive Computation of One-Loop Amplitudes*, *Comput. Phys. Commun.* **214** (2017) 140 [arXiv:1605.01090] [INSPIRE].

[26] A. Denner, S. Dittmaier and L. Hofer, *Collier: a fortran-based Complex One-Loop LIbrary in Extended Regularizations*, *Comput. Phys. Commun.* **212** (2017) 220 [arXiv:1604.06792] [INSPIRE].

[27] A. Denner and G. Pelliccioli, *Polarized electroweak bosons in W^+W^- production at the LHC including NLO QCD effects*, *JHEP* **09** (2020) 164 [arXiv:2006.14867] [INSPIRE].

[28] A. Denner and G. Pelliccioli, *NLO QCD predictions for doubly-polarized WZ production at the LHC*, *Phys. Lett. B* **814** (2021) 136107 [arXiv:2010.07149] [INSPIRE].

[29] A. Denner and G. Pelliccioli, *NLO EW and QCD corrections to polarized ZZ production in the four-charged-lepton channel at the LHC*, *JHEP* **10** (2021) 097 [arXiv:2107.06579] [INSPIRE].

[30] A. Denner, C. Haitz and G. Pelliccioli, *NLO QCD corrections to polarized diboson production in semileptonic final states*, *Phys. Rev. D* **107** (2023) 053004 [arXiv:2211.09040] [INSPIRE].

[31] M. Pellen, R. Poncelet and A. Popescu, *Polarised W+j production at the LHC: a study at NNLO QCD accuracy*, *JHEP* **02** (2022) 160 [arXiv:2109.14336] [INSPIRE].

[32] R. Poncelet and A. Popescu, *NNLO QCD study of polarised W^+W^- production at the LHC*, *JHEP* **07** (2021) 023 [arXiv:2102.13583] [INSPIRE].

[33] D.N. Le, J. Baglio and T.N. Dao, *Doubly-polarized WZ hadronic production at NLO QCD+EW: calculation method and further results*, *Eur. Phys. J. C* **82** (2022) 1103 [arXiv:2208.09232] [INSPIRE].

[34] D.N. Le and J. Baglio, *Doubly-polarized WZ hadronic cross sections at NLO QCD + EW accuracy*, *Eur. Phys. J. C* **82** (2022) 917 [arXiv:2203.01470] [INSPIRE].

[35] T.N. Dao and D.N. Le, *Enhancing the doubly-longitudinal polarization in WZ production at the LHC*, *Commun. in Phys.* **33** (2023) 223 [arXiv:2302.03324] [INSPIRE].

[36] SHERPA collaboration, *Event Generation with Sherpa 2.2*, *SciPost Phys.* **7** (2019) 034 [arXiv:1905.09127] [INSPIRE].

[37] A. Ballestrero, E. Maina and G. Pelliccioli, *W boson polarization in vector boson scattering at the LHC*, *JHEP* **03** (2018) 170 [arXiv:1710.09339] [INSPIRE].

[38] T. Gleisberg and S. Hoeche, *Comix, a new matrix element generator*, *JHEP* **12** (2008) 039 [arXiv:0808.3674] [INSPIRE].

[39] S. Dittmaier, *Weyl-van der Waerden formalism for helicity amplitudes of massive particles*, *Phys. Rev. D* **59** (1998) 016007 [hep-ph/9805445] [INSPIRE].

JHEP04(2024)001

[40] J. Alnefjord, A. Lifson, C. Reuschle and M. Sjodahl, *The chirality-flow formalism for the standard model*, *Eur. Phys. J. C* **81** (2021) 371 [arXiv:2011.10075] [INSPIRE].

[41] A. Ballestrero, E. Maina and G. Pelliccioli, *Polarized vector boson scattering in the fully leptonic WZ and ZZ channels at the LHC*, *JHEP* **09** (2019) 087 [arXiv:1907.04722] [INSPIRE].

[42] S. Höche, S. Kuttimalai, S. Schumann and F. Siegert, *Beyond Standard Model calculations with Sherpa*, *Eur. Phys. J. C* **75** (2015) 135 [arXiv:1412.6478] [INSPIRE].

[43] P. Richardson, *Spin correlations in Monte Carlo simulations*, *JHEP* **11** (2001) 029 [hep-ph/0110108] [INSPIRE].

[44] SHERPA TEAM, *Sherpa version 3.0.0 manual*, https://sherpa-team.gitlab.io/sherpa/master/index.html.

[45] S. Hoeche, F. Krauss, M. Schönherr and F. Siegert, *A critical appraisal of NLO+PS matching methods*, *JHEP* **09** (2012) 049 [arXiv:1111.1220] [INSPIRE].

[46] S. Kallweit et al., *NLO QCD+EW predictions for V + jets including off-shell vector-boson decays and multijet merging*, *JHEP* **04** (2016) 021 [arXiv:1511.08692] [INSPIRE].

[47] A. Ballestrero, E. Maina and G. Pelliccioli, *Different polarization definitions in same-sign WW scattering at the LHC*, *Phys. Lett. B* **811** (2020) 135856 [arXiv:2007.07133] [INSPIRE].

[48] C. Bierlich et al., *Robust Independent Validation of Experiment and Theory: Rivet version 3*, *SciPost Phys.* **8** (2020) 026 [arXiv:1912.05451] [INSPIRE].

[49] F. Krauss, R. Kuhn and G. Soff, *AMEGIC++ 1.0: A Matrix element generator in C++*, *JHEP* **02** (2002) 044 [hep-ph/0109036] [INSPIRE].

[50] F. Buccioni et al., *OpenLoops 2*, *Eur. Phys. J. C* **79** (2019) 866 [arXiv:1907.13071] [INSPIRE].

[51] S. Hoeche, F. Krauss, S. Schumann and F. Siegert, *QCD matrix elements and truncated showers*, *JHEP* **05** (2009) 053 [arXiv:0903.1219] [INSPIRE].

[52] S. Catani, F. Krauss, R. Kuhn and B.R. Webber, *QCD matrix elements + parton showers*, *JHEP* **11** (2001) 063 [hep-ph/0109231] [INSPIRE].

[53] S. Schumann and F. Krauss, *A parton shower algorithm based on Catani-Seymour dipole factorisation*, *JHEP* **03** (2008) 038 [arXiv:0709.1027] [INSPIRE].

[54] M. Schönherr and F. Krauss, *Soft Photon Radiation in Particle Decays in SHERPA*, *JHEP* **12** (2008) 018 [arXiv:0810.5071] [INSPIRE].

[55] G.S. Chahal and F. Krauss, *Cluster Hadronisation in Sherpa*, *SciPost Phys.* **13** (2022) 019 [arXiv:2203.11385] [INSPIRE].

[56] M. Cacciari, G.P. Salam and G. Soyez, *The anti-k_t jet clustering algorithm*, *JHEP* **04** (2008) 063 [arXiv:0802.1189] [INSPIRE].

[57] A. Buckley et al., *LHAPDF6: parton density access in the LHC precision era*, *Eur. Phys. J. C* **75** (2015) 132 [arXiv:1412.7420] [INSPIRE].

[58] NNPDF collaboration, *Parton distributions from high-precision collider data*, *Eur. Phys. J. C* **77** (2017) 663 [arXiv:1706.00428] [INSPIRE].

[59] G. Pelliccioli and G. Zanderighi, *Polarised-boson pairs at the LHC with NLOPS accuracy*, *Eur. Phys. J. C* **84** (2024) 16 [arXiv:2311.05220] [INSPIRE].

[60] NNPDF collaboration, *Parton distributions for the LHC Run II*, *JHEP* **04** (2015) 040 [arXiv:1410.8849] [INSPIRE].

JHEP04(2024)001

[61] ATLAS collaboration, *$ZZ \to \ell^+\ell^-\ell'^+\ell'^-$ cross-section measurements and search for anomalous triple gauge couplings in 13 TeV pp collisions with the ATLAS detector*, *Phys. Rev. D* **97** (2018) 032005 [arXiv:1709.07703] [INSPIRE].

[62] C. Bittrich and M. Bühring, *Rivet-Analyse for polarized same-sign WW scattering process*, https://gitlab.cern.ch/atlas-germany-dresden-vbs-group/rivet_analyses/-/tree/master/WWss/VBSCost.

[63] T. Burghardt, *Validation of polarized simulations for WZjj production in Sherpa*, BSc thesis, Institut für Kern- und Teilchenphysik (IKTP), Technische Universitat Dresden, 01069 Dresden, Germany (2022).

JHEP04(2024)001